OPEN ACCESS

Original research

Protective and aggressive bacterial subsets and metabolites modify hepatobiliary inflammation and fibrosis in a murine model of PSC

Muyiwa Awoniyi ,[1,2] Jeremy Wang,[2,3] Billy Ngo,[2] Vik Meadows,[4] Jason Tam,[5] Amba Viswanathan,[2] Yunjia Lai,[6] Stephanie Montgomery,[7] Morgan Farmer,[2] Martin Kummen ,[8,9] Louise Thingholm,[10] Christoph Schramm,[11] Corinna Bang ,[12] Andre Franke,[12] Kun Lu,[6,13] Huiping Zhou ,[14,15,16] Jasmohan S Bajaj,[14,15,16] Phillip B Hylemon,[14,15,16] Jenny Ting,[5,17] Yury V Popov ,[18] Johannes Roksund Hov ,[9,19] Heather L Francis,[20,21] Ryan Balfour Sartor [1,2,5]

► Additional supplemental material is published online only. To view, please visit the journal online (http://dx.doi.org/10.1136/gutjnl-2021-326500).

For numbered affiliations see end of article.

Correspondence to
Dr Ryan Balfour Sartor, Center for Gastrointestinal Biology and Disease, University of North Carolina System, Chapel Hill, NC 27517, USA;
ryan_balfour_sartor@med.unc.edu

Received 6 November 2021
Accepted 16 May 2022

To cite: Awoniyi M, Wang J, Ngo B, *et al*. *Gut* Epub ahead of print: [*please include* Day Month Year]. doi:10.1136/gutjnl-2021-326500

ABSTRACT

Objective Conflicting microbiota data exist for primary sclerosing cholangitis (PSC) and experimental models. Goal: define the function of complex resident microbes and their association relevant to PSC patients by studying germ-free (GF) and antibiotic-treated specific pathogen-free (SPF) multidrug-resistant 2 deficient (*mdr2*$^{-/-}$) mice and microbial profiles in PSC patient cohorts.

Design We measured weights, liver enzymes, RNA expression, histological, immunohistochemical and fibrotic biochemical parameters, faecal 16S rRNA gene profiling and metabolomic endpoints in gnotobiotic and antibiotic-treated SPF *mdr2*$^{-/-}$ mice and targeted metagenomic analysis in PSC patients.

Results GF *mdr2*$^{-/-}$ mice had 100% mortality by 8 weeks with increasing hepatic bile acid (BA) accumulation and cholestasis. Early SPF autologous stool transplantation rescued liver-related mortality. Inhibition of ileal BA transport attenuated antibiotic-accelerated liver disease and decreased total serum and hepatic BAs. Depletion of vancomycin-sensitive microbiota exaggerated hepatobiliary disease. Vancomycin selectively decreased Lachnospiraceae and short-chain fatty acids (SCFAs) but expanded Enterococcus and Enterobacteriaceae. Antibiotics increased *Enterococcus faecalis* and *Escherichia coli* liver translocation. Colonisation of GF *mdr2*$^{-/-}$ mice with translocated *E. faecalis* and *E. coli* strains accelerated hepatobiliary inflammation and mortality. Lachnospiraceae colonisation of antibiotic pretreated *mdr2*$^{-/-}$ mice reduced liver fibrosis, inflammation and translocation of pathobionts, and SCFA-producing Lachnospiraceae and purified SCFA decreased fibrosis. Faecal Lachnospiraceae negatively associated, and *E. faecalis/ Enterobacteriaceae* positively associated, with PSC patients' clinical severity by Mayo risk scores.

Conclusions We identified novel functionally protective and detrimental resident bacterial species in *mdr2*$^{-/-}$ mice and PSC patients with associated clinical risk score. These insights may guide personalised targeted therapeutic interventions in PSC patients.

WHAT IS ALREADY KNOWN ON THIS SUBJECT?

⇒ Microbiotal alterations are associated with idiopathic primary sclerosing cholangitis (PSC) but provide limited insights into functional activities and mechanisms of resident bacteria and their metabolites.
⇒ Germ-free mice and antibiotics lead to increased reuptake of bile acids, suggestive of microbial control of bile acid homeostasis.
⇒ Antibiotics have variable protective and detrimental outcomes in clinical and experimental studies but lack unified mechanistic explanations.

WHAT ARE THE NEW FINDINGS?

⇒ Germ-free mdr2$^{-/-}$ mice, a PSC murine model, exhibited 100% fatality by 8 weeks driven by lack of microbial modulation of toxic progressive hepatic and plasma bile accumulation unless rescued with faecal microbiota transfer from syngeneic specific pathogenic stool by 4 weeks of age, confirming an overall protective role of resident microbiota in this model.
⇒ Antibiotic-induced dysbiosis of specific pathogen-free (SPF) mdr2$^{-/-}$ potentiated hepatobiliary disease by non-bacteremic hepatic translocation of Enterococcus faecalis and Escherichia coli and resulted in accelerated detrimental hepatic bile acid accumulation without changing ileal FXR signalling. Inhibition of ileal bile salt transporter, Asbt, resulted in attenuated hepatic inflammation and fibrosis in antibiotic-treated SPF mdr2$^{-/-}$ mice, validating microbial modulation of bile acid homeostasis.

INTRODUCTION

Chronic biliary inflammation, cirrhosis and variable progression to liver failure characterise primary sclerosing cholangitis (PSC).[1] No current therapies exist to halt disease progression, because the mechanisms that underlie the onset and progression of PSC remain unclear. Several studies show dysbiotic microbiota in

WHAT ARE THE NEW FINDINGS?

⇒ Antibiotic-induced dysbiosis of SPF mdr2−/− potentiated hepatobiliary disease with hepatic translocation of E. faecalis and E. coli and increased bile salt hydrolase activity.

⇒ Microbial manipulations and metabolomic analysis in mdr2−/−- mice identified hepatoprotective Lachnospiraceae that inhibited pathobiont (E. faecalis and E. coli) enterohepatic translocation and mediated their anti-fibrotic effects by producing short-chain fatty acids.

⇒ In human cohorts, fecal E. faecalis/Enterobacteriaceae positively and Lachnospiraceae negatively associated with PSC clinical severity measured by Mayo risk score.

HOW MIGHT IT IMPACT ON CLINICAL PRACTICE IN THE FORESEEABLE FUTURE?

⇒ These microbial insights have the potential to better predict clinical disease courses in individual patients by assessing abundance of detrimental versus protective resident microbial populations; improving PSC faecal transplant outcomes by matching donor and recipient selection; and guiding selective microbial manipulations for personalizsed therapeutic approaches.

PSC patients with decreased microbial diversity and over-represented intestinal pathobionts like Enterobacteriaceae (*Escherichia coli* and *Klebsiella pneumonia*), Enterococcus (*Enterococcus faecalis*), *Veillonella* and biliary tract *E. faecalis*, compared with controls suggesting potential translocation.[2–5] Promotion of interleukin (IL)-17-mediated mucosal immunity play a role in PSC pathophysiology.[2 5–7] In parallel, PSC patients exhibit decreased abundance of presumed protective faecal Lachnospiraceae,[4 8] which have bile acid (BA) metabolic activities and anticolitogenic properties[9] but unclear functional hepatobiliary impact. Short-term traditional probiotic therapy (Lactobacillus and Bifidobacterium)[10] or single donor faecal microbial transfer (FMT)[11] are ineffective for PSC patients, possibly related to no native colonisation of these bacteria.[3 4 8] These studies indicate the complexity and strong association of microbiota with PSC and illustrate the need for further understanding of pathogenic and protective roles of resident gut microbiota.

Preclinical studies document the protective role of unfractionated gut microbiota in experimental PSC. In both chemically induced[12] and genetic (FVB/N *mdr2*$^{-/-}$)[13] murine PSC models, germ-free (GF) mice exhibited accelerated liver disease compared with conventionally raised controls. GF conditions lead to extensive reuptake of intestinal BAs,[12] emphasising the importance of microbial mediation of BA homeostasis. Microbial depletion expands hepatic non-micellar BA concentrations contributing to cholangiocyte inflammation, ductal disruption and parenchymal disease in *mdr2*$^{-/-}$ mice.[13–15] Dysbiosis in PSC patients results in altered BA pools that potentially contribute to PSC pathophysiology.[3 14] Furthermore, increased microbial bile salt hydrolase (BSH) activity was found in PSC patients' bile,[3] possibly related to the high BSH activity of *E. faecalis*, abundant in the faeces and bile of PSC patients.[3 4 16 17] These observations suggest a potential pathogenic role for bacterial BSH activity in PSC. Functional microbial or metabolic studies are needed to further delineate mechanistic differences among intestinal bacteria that differentially influence hepatobiliary damage, inflammation and fibrosis in PSC.

In this study, we used gnotobiotic and antibiotic approaches in specific pathogen-free (SPF) *mdr2*$^{-/-}$ mice to study the functional roles of resident bacteria in cholestatic liver disease. We identified functionally protective (Lachnospiraceae) and pathogenic (*E. faecalis* and *E. coli*) resident bacteria and defined in vivo mechanisms through complementation studies. Conserved relative abundance of these bacteria was found in metagenomic analysis of PSC patient faeces with a moderate association with Mayo clinical risk score in PSC patients denoting parallel microbial roles in experimental and clinical disease. These insights could target donor selection in future PSC-FMT trials and guide selective faecal enrichment/depletion approaches to increase efficacy of future personalised microbial therapies.

METHODS

Ethics statement/animal husbandry

The Popov lab generated C57Bl/6 SPF *mdr2(abcb4)*$^{-/-}$ mice.[18] *Mdr2*$^{-/-}$ and WT SPF control C57BL/6 mice were housed in vivaria microisolator cages with no more than five mice/cage or in GF Trexlar isolators. The UNC National Gnotobiotic Rodent Resource Center derived GF *mdr2*$^{-/-}$ mice by caesarian section. We bred GF *mdr2*$^{+/-}$±mice due to early mortality of GF *mdr2*$^{-/-}$ mice. Age-matched and sex-matched mice had unrestricted access to autoclaved water and 5v0F Purina LabDiet chow with a 12-hour light/dark cycle. Human microbiome data were analysed from a previous study.[4]

Antibiotic treatments

Non-fasted 3–4 week old male and female mice received either combined or single antibiotics (0.5 mg/mL vancomycin (Hospira), 1 mg/mL neomycin (Medisca) and 50 mg/kg metronidazole (G.D. Searle)) in drinking water ad libitum, consuming 6–7 mL/mouse/day.[19 20] The antibiotic mixture was diluted in deionised H_2O, sterilised through a 0.2 µm filter and replaced twice weekly for 7–14 days.

Patient and public involvement

No involvement.

Statistical analysis

Murine data are shown as mean±SEM, with 'n' representing number of mice indicated in figure legends. One dot represents one mouse. Linear fitting and normalisation were performed in GraphPad Prism. Unless specified in the figure legends, statistical significance between two groups was determined by unpaired, two-tailed Student's t-test; significance between >2 groups determined using one-way analysis of variance with Fisher's LSD test using GraphPad Prism default settings. We compared CFU numbers by the Poisson generalised linear model, estimated with a Markov Chain Monte Carlo method robust for small sample sizes. Error bar represents mean±SEM with *p<0.05, **p<0.01, ***p<0.001, ****p<0.0001 and n.s. as no significance. Further details of histological staining, IHC staining and analysis, bacterial or metabolite inoculation, cultivation and translocation, biochemical, liver enzyme, metabolomic and 16S rRNA sequencing/analysis are presented in the online supplemental material and methods.

RESULTS

Autologous stool transplant alleviate the non-micellular hepatic BA accumulation, hepatobiliary inflammation, fibrosis and mortality in germ-free *mdr2*$^{-/-}$ mice

To evaluate resident microbiota's role in this experimental cholestatic murine model, we generated and characterised GF C57BL/6 *mdr2*$^{-/-}$ mice compared with littermate C57BL/6 WT mice. Relative to SPF conditions, 6–7 week old GF *mdr2*$^{-/-}$ mice had decreased weight gain, 2× increased alkaline phosphatase

(ALP) and 15× increased total bilirubin (TB) (figure 1A–C). GF *mdr2*$^{-/-}$ mice from weaning 5 weeks had histologically normal livers (data not shown) and normal TB (figure 1C). Rapid onset of cholestasis in GF *mdr2*$^{-/-}$ occurred beyond age 6 weeks, not seen in age-matched SPF *mdr2*$^{-/-}$ mice, in GF WT C57BL/6 or older GF *mdr2*$^{+/-}$ ± (≤70 weeks) (figure 1C, online supplemental figure S1A,D). Loss of microbiota in *mdr2*$^{-/-}$ mice resulted in >3–5 fold progressively increased hepatic and serum BAs strongly correlating with body mass wasting and biomarkers of cholestatic injury (figure 1C–E). Most hepatic BA were 1°BA (cholic and muricholic acids, S1B-C). GF *mdr2*$^{-/-}$ and wild-type (WT) C57BL/6 mice exhibited elevated hepatic BA, attenuated liver cyp7a1 gene expression (figure 1E, online supplemental figure S1H) despite no difference in ileal ASBT, FXR or FGF15 (figure 1G, online supplemental figure S1E–G) compared with SPF controls.

GF *mdr2*$^{-/-}$ had increased hepatic RNA expression of IL-17/IL-22 master regulator, Rorγt and inflammatory cytokine *TNF-α* (figure 1H,I). Total hepatic hydroxyproline content, a collagen biochemical marker, was increased in GF *mdr2*$^{-/-}$ mice, along with RNA expression of fibrinogenic markers, *co1α1* and *timp-1* (figure 1J–L). GF and SPF *mdr2*$^{-/-}$ mice developed hepatomegaly versus WT controls (online supplemental figure S1F).

GF *mdr2*$^{-/-}$ mice had markedly decreased survival (median mortality 7.5 weeks and 100% mortality by 8 weeks) compared with SPF *mdr2*$^{-/-}$ mice (figure 1N). Faecal transplantation (FMT) of SPF *mdr2*$^{-/-}$ faeces to 3–4 week old GF *mdr2*$^{-/-}$ mice improved survival (75% at 400 days; figure 1N) and decreased TB (figure 1P) 2 weeks post-transplant. FMT later in life (5.5–7 weeks) provided no protection (figure 1N). Although both SPF and GF female *mdr2*$^{-/-}$ mice developed more prominent periportal inflammation relative to males, mortality was not sex related in GF *mdr2*$^{-/-}$ mice. FMT did not affect mortality in GF *mdr2*$^{+/-}$, SPF *mdr2*$^{-/-}$ or WT mice (online supplemental figure S1J).

GF *mdr2*$^{-/-}$ mice displayed heightened periportal inflammation, periductular macrophages, centrilobular necrosis and ductular proliferation (figure 2A,B and E,F) and more pronounced macrophage (figure 2C–D) than neutrophilic (S1K-L) infiltration versus SPF *mdr2*$^{-/-}$ mice. SPF *mdr2*$^{-/-}$ mice displayed more prominent sinusoidal macrophage distribution compared with periductular localisation in GF mice, whereas SPF donor FMT-treated GF *mdr2*$^{-/-}$ had a mixed phenotype. Notable hepatic lesions (figure 2A, E and G, arrows) range from hepatocytes with vacuolar and cystic degeneration to coagulation necrosis rimmed by inflammation. The cause of these lesions is not apparent, but a similar lesion has been reported in biliary ligation[21] and antibiotic-induced cholestatic[14] studies to be the result of bile salt leakage and described as bile infarcts. in GF *mdr2*$^{-/-}$ mice. SPF *mdr2*$^{-/-}$ mice developed periductal fibrosis with focal parenchymal extensions, but GF *mdr2*$^{-/-}$ mice had doubled histological fibrosis scores with extensive periductal fibrosis extending well into the parenchyma with frequent bridging to portal veins, resembling stage 3–4 Ishak fibrosis patterns (figure 2G). Early FMT attenuated periportal inflammation and fibrosis in GF *mdr2*$^{-/-}$ mice (figure 2B and H). No histological hepatic or ileocolonic inflammation occurred in GF or SPF WT or *mdr2*$^{+/-}$ ± (data not shown). Thus, early life exposure to resident microbiota in GF *mdr2*$^{-/-}$ mice promotes survival and decreased hepatic inflammation, ductular reaction and fibrosis.

mdr2$^{-/-}$ mice have dysbiotic microbial landscapes with altered metabolic pathways exacerbated by antibiotics

Resident faecal microbial community structure diverged in SPF *mdr2*$^{-/-}$ and WT mice by β-diversity analysis (figure 3A) with decreased putative protective Clostridial family abundance (figure 3B). To validate the protective role of host–microbiota and identified potential beneficial bacterial groups and metabolites, we developed an antibiotic depletion model in SPF *mdr2*$^{-/-}$ mice via administration of a broad-spectrum antibiotic cocktail (Abx) targeting resident Gram-positive, Gram-negative and anaerobic bacteria[19 20] for 14 days (figure 3C). As predicted, Abx similarly depleted microbial abundance in *mdr2*$^{-/-}$ and WT control mice by α-diversity and faecal qPCR (figure 3D–G). *β*-diversity analysis demonstrated markedly different microbial communities in the two hosts following Abx (figure 3H,I).

To identify potential metabolic profiles reflecting protective microbial effects in *mdr2*$^{-/-}$ mice, we analysed the metabolome of serum and cecal contents from Abx-treated versus untreated *mdr2*$^{-/-}$ mice by liquid chromatography-mass spectrometry (LC/MS) (figure 3J–L). Abx decreased multiple compounds, spanning BA, alcohols, indoles, oxosteroids, bilirubin and methyl-branched fatty acid pathways (figure 3L). We used these metabolomic profiles to identify putative functional properties of protective bacterial candidates, Clostridiaceae and Lachnospiraceae that might rescue inflammation/fibrosis driven by Abx depletion of protective microbial subsets.

Antibiotic depletion of resident microbiota augments intestinal permeability, liver inflammation, biliary epithelial reactivity and fibrosis and restricts weight gain in *mdr2*$^{-/-}$ mice

Abx markedly depleted putative protective Clostridiaceae and Lachnospiraceae families (figure 4B) and increased intestinal permeability versus WT mice (figure 4C). Weight loss in *mdr2*$^{-/-}$ mice limited Abx treatment to 14 days (figure 4D) with increased serum ALP and clinical illness (lethargy, hunching, unkempt fur and peritoneal jaundice), and minimal serum bilirubin elevation (figure 4E,F), not seen in Abx-WT mice (online supplemental figure S1M–O). Like GF *mdr2*$^{-/-}$ mice, Abx-induced inflammation increased hepatic *Tnf-α* expression (figure 4G). Histological evaluation of Abx-treated *mdr2*$^{-/-}$ displayed accelerated cholangiopathic injury similar to GF *mdr2*$^{-/-}$ mice with expanded portal/peribiliary inflammation and ductular reaction (figure 4K–N).

Abx-treated *mdr2*$^{-/-}$ mice developed increased bridging fibrosis compared with untreated SPF *mdr2*$^{-/-}$ mice (figure 4O–P). Unchanged hydroxyproline content (figure 4H) was likely due to the short study duration, but increased liver RNA expression of *co1α1* and *timp-1* occurred in Abx-treated *mdr2*$^{-/-}$ mice versus untreated controls (figure 4I,J). This Abx depletion validated our GF *mdr2*$^{-/-}$ findings, confirming that decreased protective resident bacteria potentiates disease in this cholestatic model.

Ileal BA transport inhibition attenuates hepatic BA pool size and hepatobiliary inflammation/cholestasis in antibiotic treated *mdr2*$^{-/-}$ mice

To test mechanistic interventions, we identified the shortest duration of Abx therapy that accelerated hepatobiliary inflammation/fibrosis but maintained a 2-week experimental window for microbial transfer experiments. Interestingly, the shorter 7-day treatment enhanced hepatic inflammation and ALP elevation (online supplemental figure S2B, C) versus 14-day

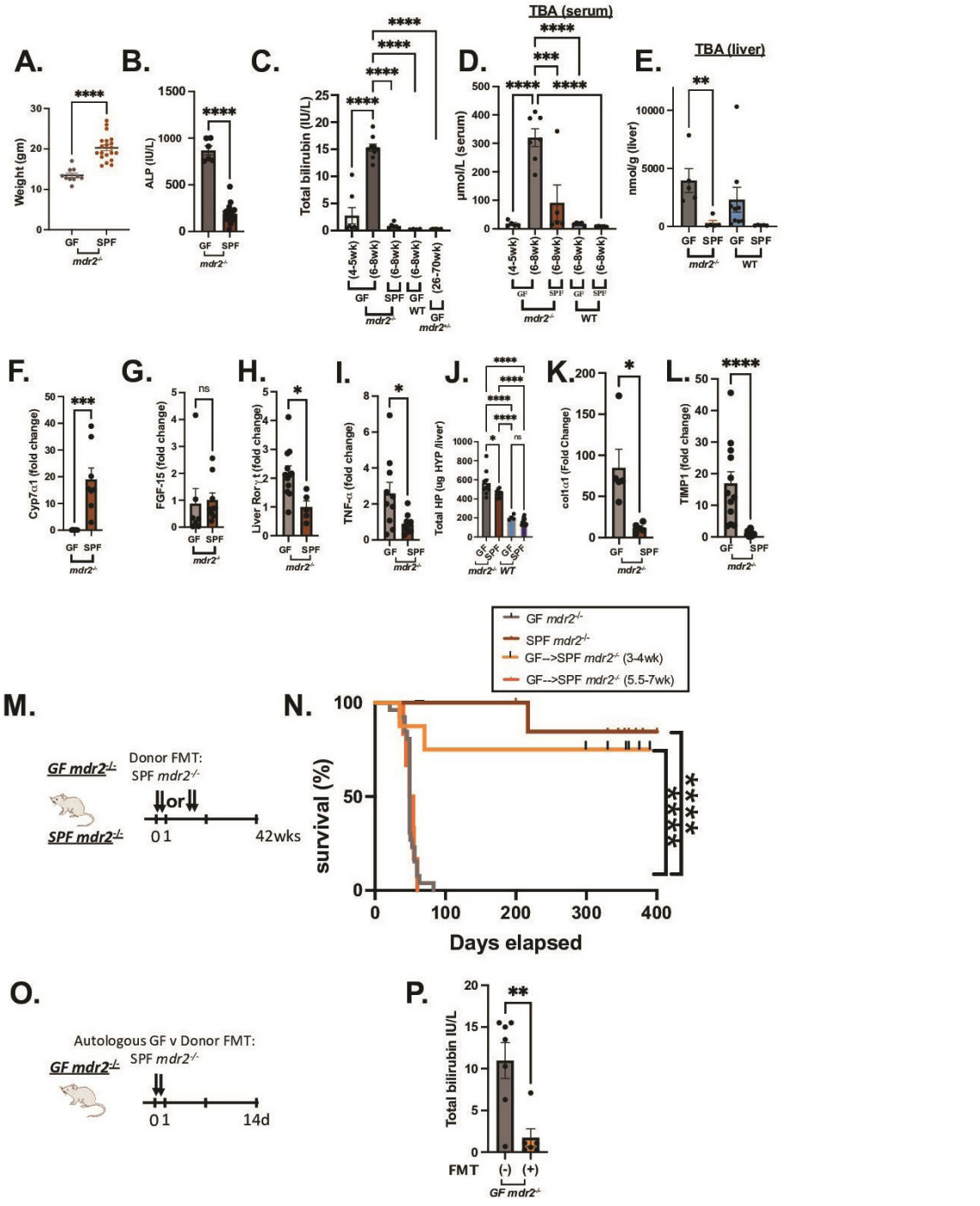

Figure 1 Clinical, biochemical and liver histological indicators of germ-free (GF) *mdr2*$^{-/-}$ mice with or without faecal microbiotal transplant compared with control mice. Mouse body weight (A) and serum alkaline phosphatase (AP), (B) of 6–8 week old GF (n=6–10) and SPF (n=20) *mdr2*$^{-/-}$ mice. Longitudinal total bilirubin (TB) (C) or total serum bile acids (TBA) (D) assessment in GF *mdr2*$^{-/-}$ mice from 4–5 week old (n=7) to 6–8 week old (n=8), compared 6–8 week old SPF *mdr2*$^{-/-}$ and C57/BL6 WT GF mice and older (26–70 week old) *mdr2*$^{+/-}$ ±. Total liver bile acids (Bas) in *mdr2*$^{-/-}$ or WT mice in GF or SPF environments (E, n=5–9/mice per group). Liver cyp7a1 expression (F) and liver FGF-15 expression (G). Relative expression (fold change) of liver cyp7a1, terminal Ileal FGF-15, Rorγt and *tnf-α* (F–I) of 6–8 week old GF (n=5–7) and SPF (n=5–7) *mdr2*$^{-/-}$ mice. Hepatic collagen deposition expressed as total hepatic hydroxyproline (HYP) expressed in ug HYP/whole liver, calculated by multiplying individual liver weight with relative HYP content (J). Relative expression (fold change) of collagen I alpha-1 (*col1α1*) and tissue inhibitor of metalloproteinases (TIMP) 1 (K–L) in livers of 6–8 week old GF (n=5–12) and SPF (n=5–8) *mdr2*$^{-/-}$ mice. Experimental design of autologous faecal microbiota transplant (FMT) study (M) Kaplan-Meyer survival curves of pooled SP *mdr2*$^{-/}$ donor stool orally gavaged into GF *mdr2*$^{-/-}$ C57Bl/6 mice twice in the first 2 days at age 3–4 weeks (n=8) or 5.5–7 weeks (n=6) compared with untreated GF (n=23) or SPF (n=14) *mdr2*$^{-/-}$ mice monitored for survival for 42 weeks (N). Experimental design of GF *mdr2*$^{-/-}$ given autologous GF (n=7) or SPF donor (n=6) stool for 14 days (O) monitoring serum TB (P). Results are expressed as means±SEM. Survival data are analysed by log-rank (Mantel-Cox) test, group or pairwise comparisons performed by analysis of variance or Student's t-test, respectively. Welch correction was applied to histological scoring analysis. *P<0.05, **p<0.01, ***p<0.001, ****p<0.0001. SPF, specific pathogen free.

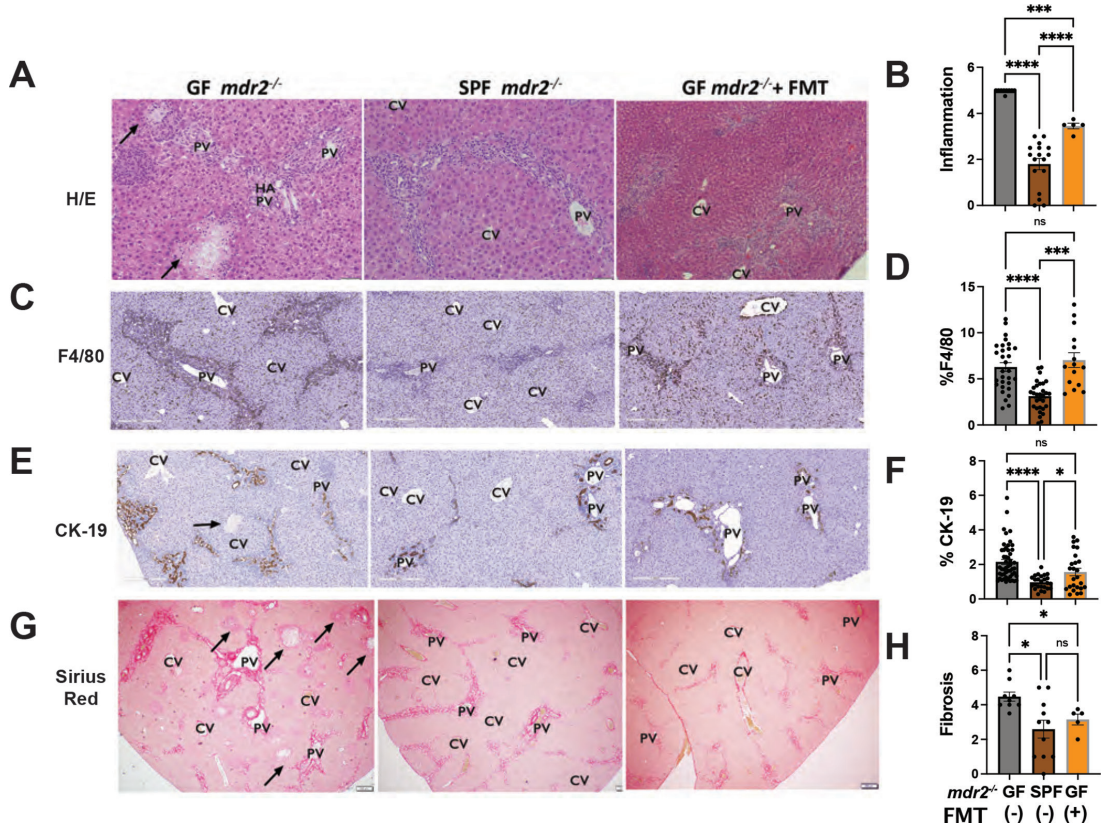

Figure 2 Histological impact of absent and reconstitution of resident microbes in GF *mdr2*$^{-/-}$ mice. Representative photomicrographs of 6–8 week old GF *mdr2*$^{-/-}$ mice±faecal microbiota transplant at 3–4 week old compared with age-matched SPF *mdr2*$^{-/-}$ mice with blinded scoring for liver inflammation (A and B), macrophages (4-4/80 immunohistochemical staining) (C and D), ductular reaction (CK-19 immunohistochemical staining) (E and F) and fibrosis (G and H) stained by H&E (200×), antibodies to F4/80 (200×) and CK-19 (200×), and Sirius Red (100×), respectively. Arrows indicate foci of hepatocyte degeneration and necrosis bordered by inflammation (bile infarct). CK-19 staining in panels D and F count positive cells in five high powered fields/ slide. Results are expressed as means±SEM. Group or pairwise comparisons were performed by analysis of variance or Student's t-test, respectively. Welch correction was applied to histological scoring analysis. *P<0.05, **p<0.01, ***p<0.001, ****p<0.0001. CV, central vein; PV, portal vein.

treatment, without significantly altering fibrosis scores (online supplemental figure S2D,E).

To further investigate the role of microbial-mediated altered BA pool size and hepatobiliary disease in this model, we identified effects of an apical sodium-dependent bile acid inhibitor (ASBTi) in our accelerated antibiotic model (figure 5A). ASBTi restored age-appropriate weight gain and attenuated cholestasis, inflammation and fibrosis (figure 5B,C and G,H, online supplemental figure S2F). Abx increased serum TBA hepatic shunting, like GF mice, that was attenuated by ASBTi (figure 5D). The predicted ASBTi-induced increased faecal BA was sustained for the 2-week treatment (figure 5I). Compensatory induction of the cyp7a1 metabolite, hepatic C4 (figure 5E,F), supported the trending decreased hepatic BA pool. Additionally, we found increased faecal primary unconjugated BAs (cholic acid (CA) and muricholic acid (MCA) (figure 5I–K). These studies indicate that resident bacterial depletion elevates non-micellular BA hepatobiliary toxicity in susceptible mice, mediated by enterohepatic BA transport.

Selective antibiotics have differential effects on *mdr2*$^{-/-}$ hepatobiliary disease

To identify microbial populations responsible for protecting *mdr2*$^{-/-}$ mice, we tested individual Abx components: vancomycin, neomycin and metronidazole that target Gram-positive, Gram-negative and anaerobic bacteria, respectively (figure 6A). Vancomycin most significantly decreased faecal bacterial α-diversity (figure 6B) and maintained most divergent bacterial populations with maximum β-diversity separation from untreated controls (figure 6C). Vancomycin and metronidazole decreased putative protective Clostridiaceae, but only vancomycin attenuated Lachnospiraceae. Neomycin did not significantly affect either family (figure 6D). Vancomycin treatment did not affect total serum BA levels (figure 6G), similar to Abx, but restricted weight gain and elevated serum ALP, hepatic TNF-αexpression, histological inflammation and ductal reaction (figure 6E,F and H–J).

Concurrent with hepatobiliary injury and inflammation, vancomycin exacerbated hepatic fibrogenesis. Relative to control mice, only vancomycin significantly increased histological liver fibrosis scores (figure 6N), hepatic profibrotic *co1α1* and *timp-1* expression (figure 6L,M) but not hepatic hydroxyproline (figure 6K).

Exploration of selective Abx on BA metabolism demonstrated isolated metronidazole attenuated hepatic *cyp7a1* expression in SPF *mdr2*$^{-/-}$ mice (figure 6O). Vancomycin profoundly increased BSH activity, measured by the unconjugated/conjugated BA ratio (figure 6P), despite not changing total faecal BAs versus control (figure 6R). These results suggest that depletion of vancomycin-sensitive bacterial populations, including Clostridiaceae and Lachnospiraceae, results in aggressive hepatobiliary responses.

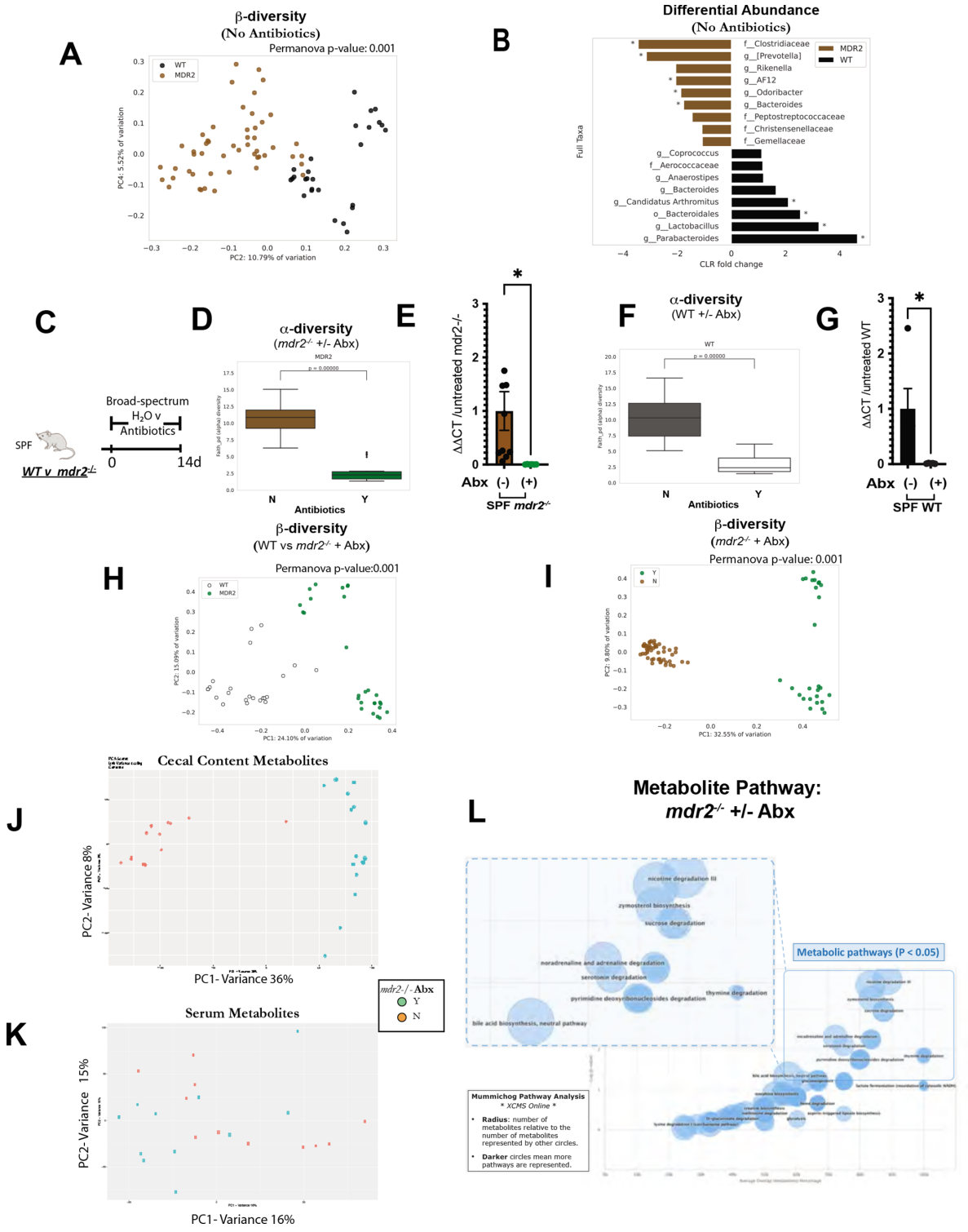

Figure 3 Faecal microbiome and metabolite profiles of preantibiotic/postantibiotic treated *mdr2*$^{-/-}$ and wild-type (WT) mice on C57BL/6 background. Pooled baseline untreated SPF *mdr2*$^{-/-}$ and WT C57BL/6 16S sequencing faecal beta diversity (Permanova test) (A) and linear discriminant analysis plot showing differential enrichment of taxa (B). Experimental design of broad-spectrum antibiotic (Abx) study, 3–5 week old SPF *mdr2*$^{-/-}$ or WT mice exposed ad libitum to broad-spectrum antibiotics (metronidazole: 30 mg/mL; vancomycin: 0.5 mg/mL; and neomycin: 1 mg/mL) in drinking H_2O or H_2O alone (n=10 mice/group) for 14 days (pooled from three experiments) (C). Effect of 14 days of Abx assessing pooled baseline alpha diversity (Faith's PD) and faecal universal 16S qCR (expressed in ΔΔCT differences) in *mdr2*$^{-/-}$ (D and E) and WT BL/6 (F and G) mice, respectively. Principal coordinates analysis (PcoA) plots assessing beta diversity (Permanova test) antibiotic exposure between genotypes (WT and *mdr2*$^{-/-}$ mice) (H) and antibiotic exposure in *mdr2*$^{-/-}$ mice (I). 3D-PCA plot shows the separation of cecal (J) and serum (K) metabolites from *mdr2*$^{-/-}$ with and without antibiotics. Mummichog pathway cloud plot of potential pathway differences with exposure of broad antibiotics in SPF *mdr2*$^{-/-}$ mice (L). The radius of each circle represents the number of metabolites relative to the number of metabolites represented by other circles. Darker circles mean more pathways are represented (*mdr2*$^{-/-}$ no Abx: n=13, *mdr2*$^{-/-}$ with Abx: n=25). Group or pairwise comparisons performed by analysis of variance or Student's t-test, respectively. *P<0.05, **p<0.01, ***p<0.001, ****p<0.0001. SPF, specific pathogen free.

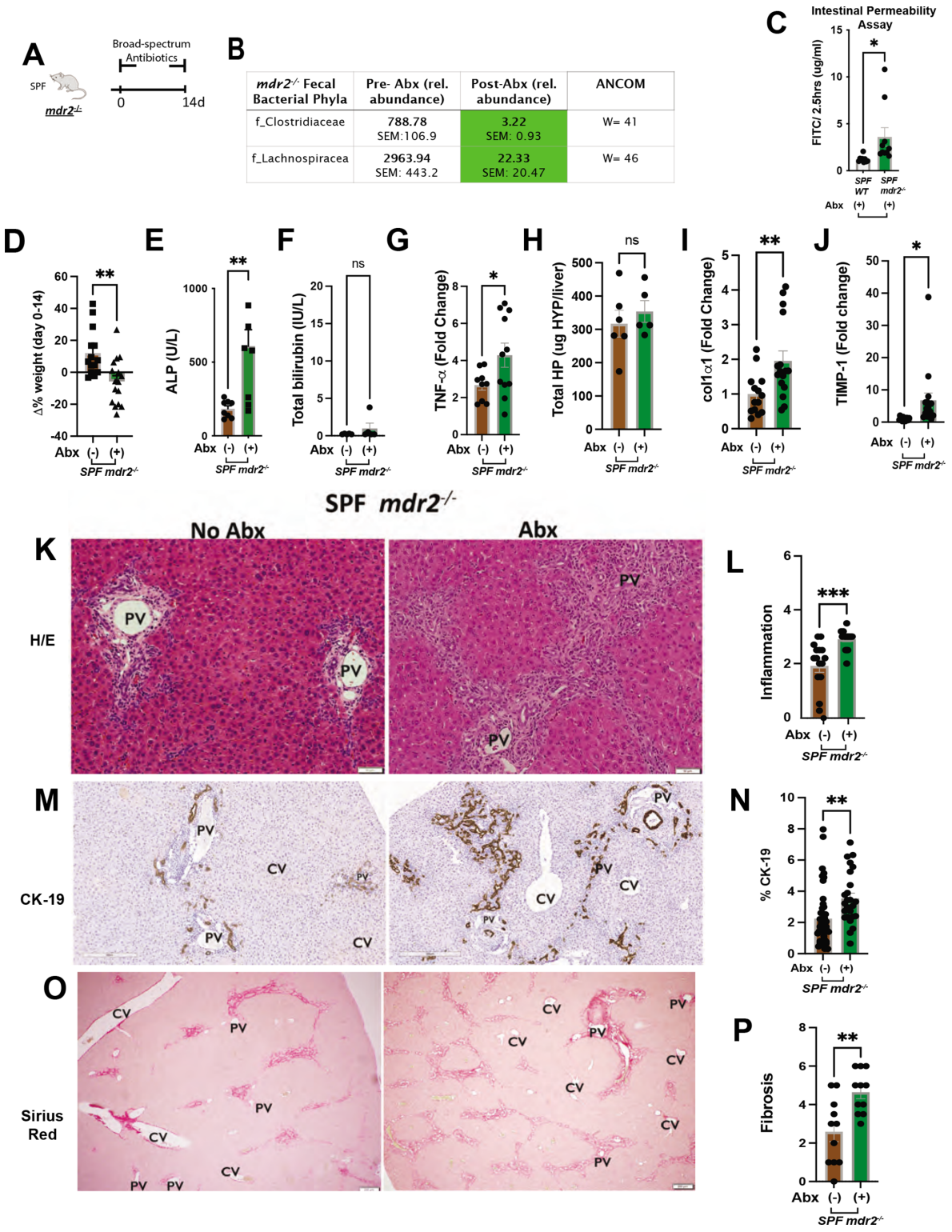

mdr2$^{-/-}$ Fecal Bacterial Phyla	Pre- Abx (rel. abundance)	Post-Abx (rel. abundance)	ANCOM
f_Clostridiaceae	788.78 SEM:106.9	3.22 SEM: 0.93	W= 41
f_Lachnospiracea	2963.94 SEM: 443.2	22.33 SEM: 20.47	W= 46

Figure 4 Clinical, biochemical and liver histological indicators of broad-spectrum antibiotic treated *mdr2*$^{-/-}$ mice. Experimental design of broad-spectrum antibiotic (Abx) study, 3–5 week old SPF *mdr2*$^{-/-}$ mice exposed ad libitum to broad-spectrum antibiotics in drinking H_2O (n=15) or H_2O alone (n=13) for 14 days (pooled from three experiments) (A). Effect of Abx exposure on various outcomes including relative abundance of selected bacterial phyla expressed as unadjusted raw average operational taxonomic unit (OTU) relative abundance (B), colonic/TI permeability (WT & *mdr2*$^{-/-}$ mice) (C), 14 days body weight change (D), serum ALP, TB (E and F), RNA expression of liver *tnf*-α (G), *col1α1* (I) and *timp*-1 (J) and hepatic collagen deposition expressed as ug HYP/whole liver (H). Representative photomicrographs and blinded composite histological scoring murine liver stained with H&E (K–L), CK-19 (M–N) and Sirius Red (O–P) of untreated (n=15) versus Abx-treated SPF *mdr2*$^{-/-}$ mice (n=15). Results are expressed as means±SEM. Pairwise comparisons were performed by Student's t-test for biochemical and molecular studies; Welch correction was applied to histological scoring analysis. Unadjusted raw average OTU relative abundance and SEs of bacterial groups against the variables detected with significant effects by analysis of composition of microbes). *P<0.05, **p<0.01, ***p<0.001. ALP, alkaline phosphatase; SPF, specific pathogen free; TB, total bilirubin.

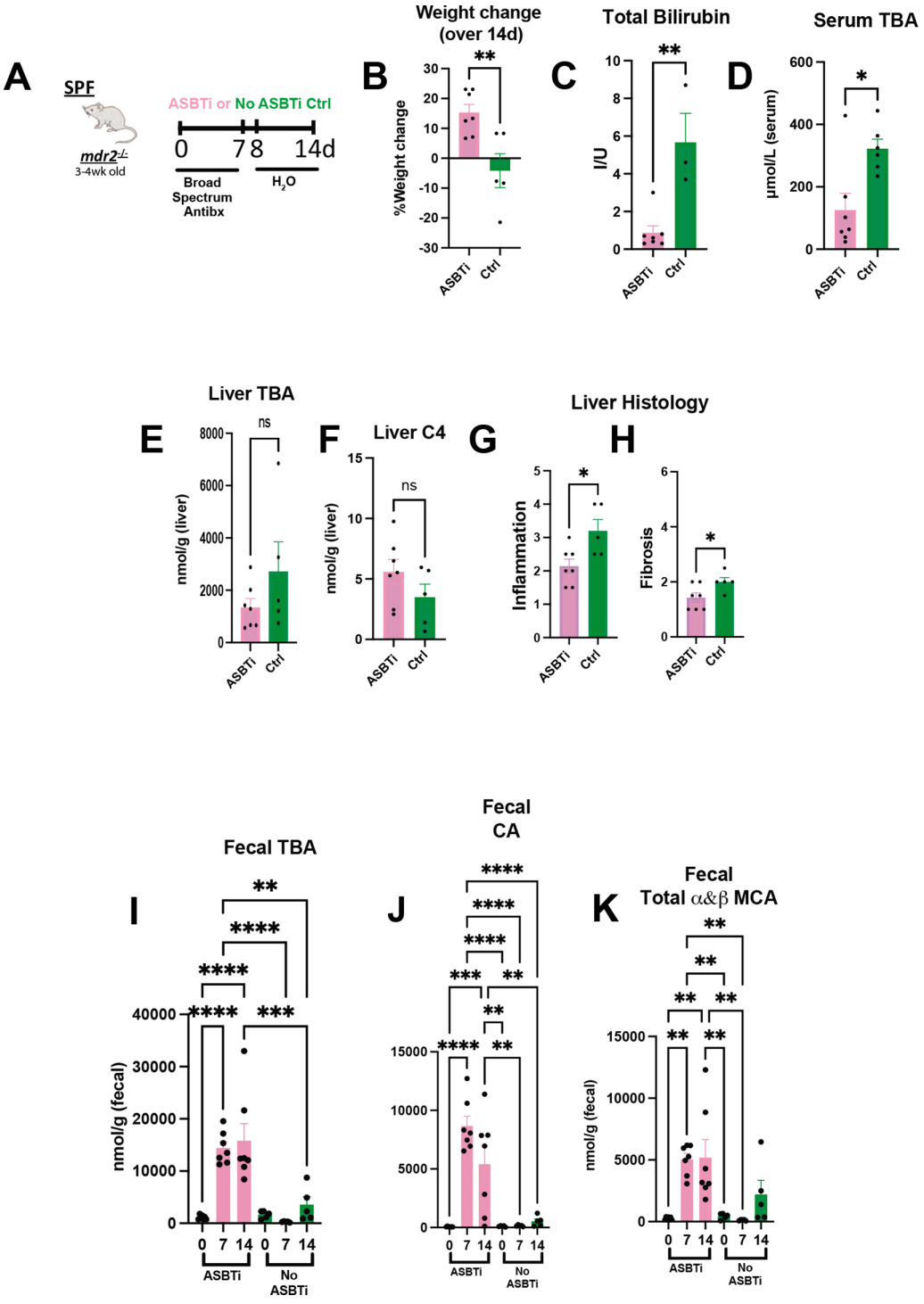

Figure 5 Bile acid homeostasis and hepatobiliary injury assessed in Abx treated *mdr2*$^{-/-}$ mice following ASBT blockage. Experimental design of ad libitum exposure in drinking H_2O of ASBT inhibitor (GSK23306, 10 mg/kg) for 14-day concomitant with 7-day broad antibiotic pretreatment in 4–5 week old SPF *mdr2*$^{-/-}$ mice versus no ASBTi (water only) group (n=5–7 mice/group) (A). Effect of ASBT inhibition on: weight change (B), TB (C), serum and liver total BA (D–E), liver C4 (F, metabolite of Cyp7a1 activation), histological liver inflammation and fibrosis (G and H). Assessment of longitudinal faecal bile acid homeostasis at times 0, 7 and 14 days following initiation of ASBT inhibition evaluating TBA, cholic acid (CA) and α+β MCA (I–K). Group or pairwise comparisons performed by analysis of variance or Student's t-test, respectively. *P<0.05, **p<0.01, ***p<0.001, ****p<0.0001. ASBTi, apical sodium-dependent bile acid inhibitor; SPF, specific pathogen free; TB, total bilirubin.

Lachnospiraceae administration attenuates phenotypic effects of antibiotic-treated SPF *mdr2*$^{-/-}$ mice and inhibits hepatic bacterial translocation

We reconstituted the putative protective bacteria, Clostridiaceae and Lachnospiraceae, in the accelerated 7d Abx model (online supplemental figure S2A–E). Because Abx depleted protective faecal Clostridium clusters IV and XIVa[22 23] in both SPF WT and *mdr2*$^{-/-}$ mice (online supplemental figure S2K,L), we initially tested a 17-strain consortium of protective human Clostridia.[22] Despite efficacy of these Clostridium strains in multiple colitis

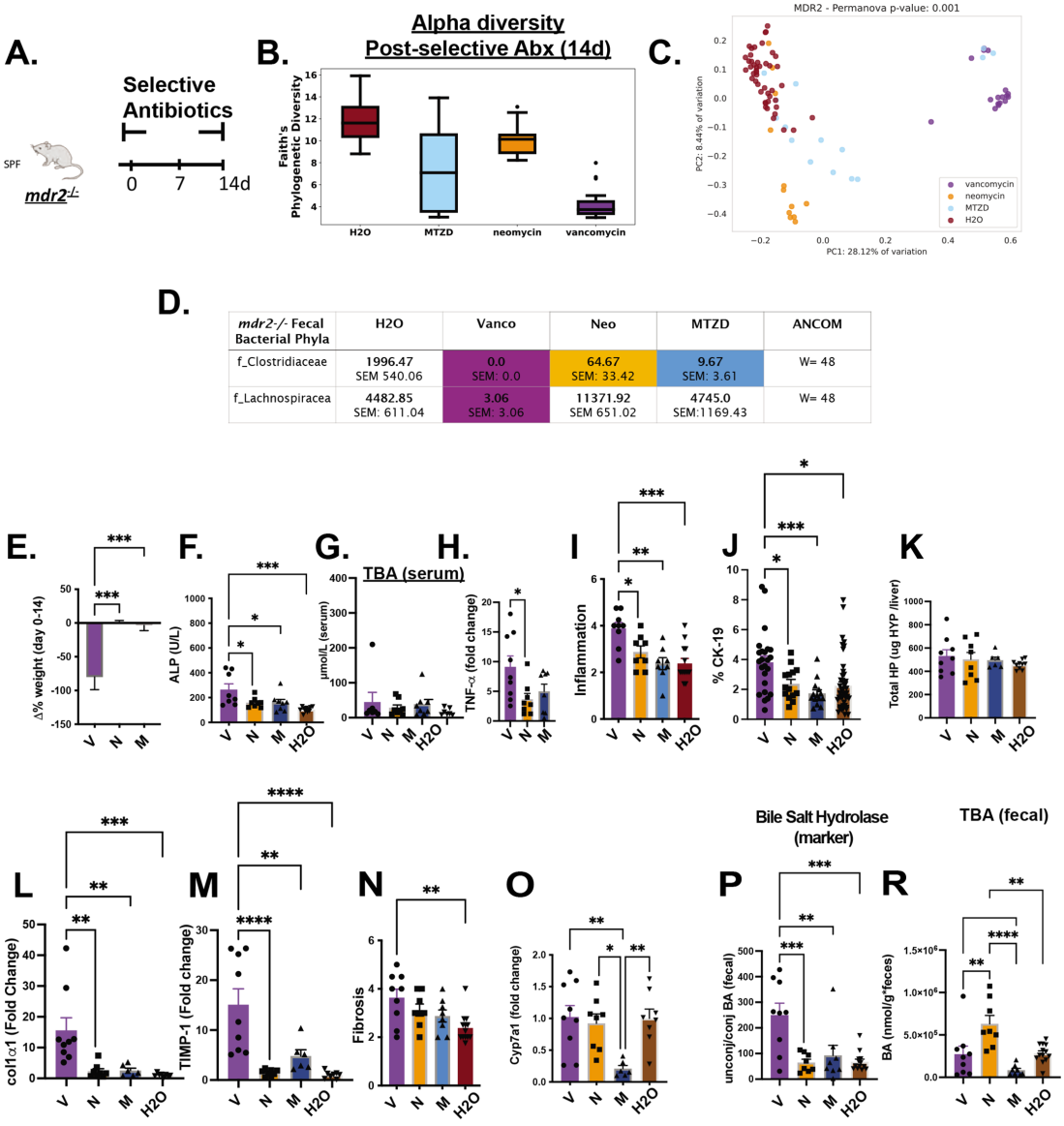

Figure 6 Differential effects of selective antibiotics on *mdr2*$^{-/-}$ microbial, clinical, biochemical and histological outcomes. Experimental design of selective antibiotic treatment (A): SPF *mdr2*$^{-/-}$ mice were given individual antibiotics (vancomycin (V; 0.5 mg/mL, n=16), neomycin (N; 1 mg/mL, n=12) or metronidazole (M; 30 mg/mL, n=16) in autoclaved drinking water ad libitum and control *mdr2*$^{-/-}$ mice received autoclaved water alone (n=16) for 14 days. Alpha diversity, beta diversity (Permanova test) and differential abundance (centred log-ratio (CLR) transformation from CoDA methods) of Clostridiaceae and Lachnospiraceae from 14d faecal samples (B–D). Measured parameters include: 14-day weight change (E), serum ALP (F) and serumtotal bile acids (TBA) (G), and liver RNA expression of *tnf*-α (H); along with blinded composite histologic scoring murine liver stained with H&E (I) and CK-19 (J). Fibrosis readouts include hepatic collagen deposition (K), RNA expression of *col1α1* (L) and *timp*-1 (M) along with Sirius Red composite staining (N) *cyp7a1* liver expression (O) as well as pooled cecal content bile acids (BAs) differences in surrogate bile salt hydrolase activity indicator based on ratios of total unconjugated/conjugated BA (P) and total BA (R) of selective antibiotic treated *mdr2*$^{-/-}$ compared with H_2O control. (V=9, N=8, M=8, H_2O=8). CK-19+ represented of 5HPF/liver/mouse. Group or pairwise comparisons performed by analysis of variance or Student's t-test, respectively. Welch correction was applied to histological scoring analysis. Unadjusted raw average OTU relative abundance and SEs of bacterial groups against the variables detected with significant effects by analysis of composition of microbes. *P<0.05, **p<0.01, ***p<0.001, ****p<0.0001. ALP, alkaline phosphatase; SPF, specific pathogen free.

models,[22] their repletion in antibiotic-pretreated *mdr2*$^{-/-}$ mice did not alter body weight or liver enzymes (online supplemental figure S2M–P). Therefore, we assessed the biological activity of potentially protective Lachnospiraceae also depleted by Abx and vancomycin (figure 6D). Serial treatment with a protective colonic 23 strain Lachnospiraceae consortium (Lachno)[24] (figure 7A) restored weight gain and reduced histological liver inflammation, ductular reaction and fibrosis (figure 7B and E–G) but did not decrease serum biochemistries (figure 7C, online supplemental figure S2Q). Lachno exposure minimally affected total faecal and serum BA, liver cyp7a1 and ileal FGF15 gene expression (online supplemental figure S2R–U). Reconstituting Lachnospiraceae in GF *mdr2*$^{-/-}$ mice resulted in reduced liver fibrosis, without affecting mortality or liver inflammation compared with non-colonised GF *mdr2*$^{-/-}$ mice (online supplemental figure S3F–H).

Abx altered faecal microbial communities 7 days after treatment with expanded Ruminococcaceae, Enterobacteriaceae

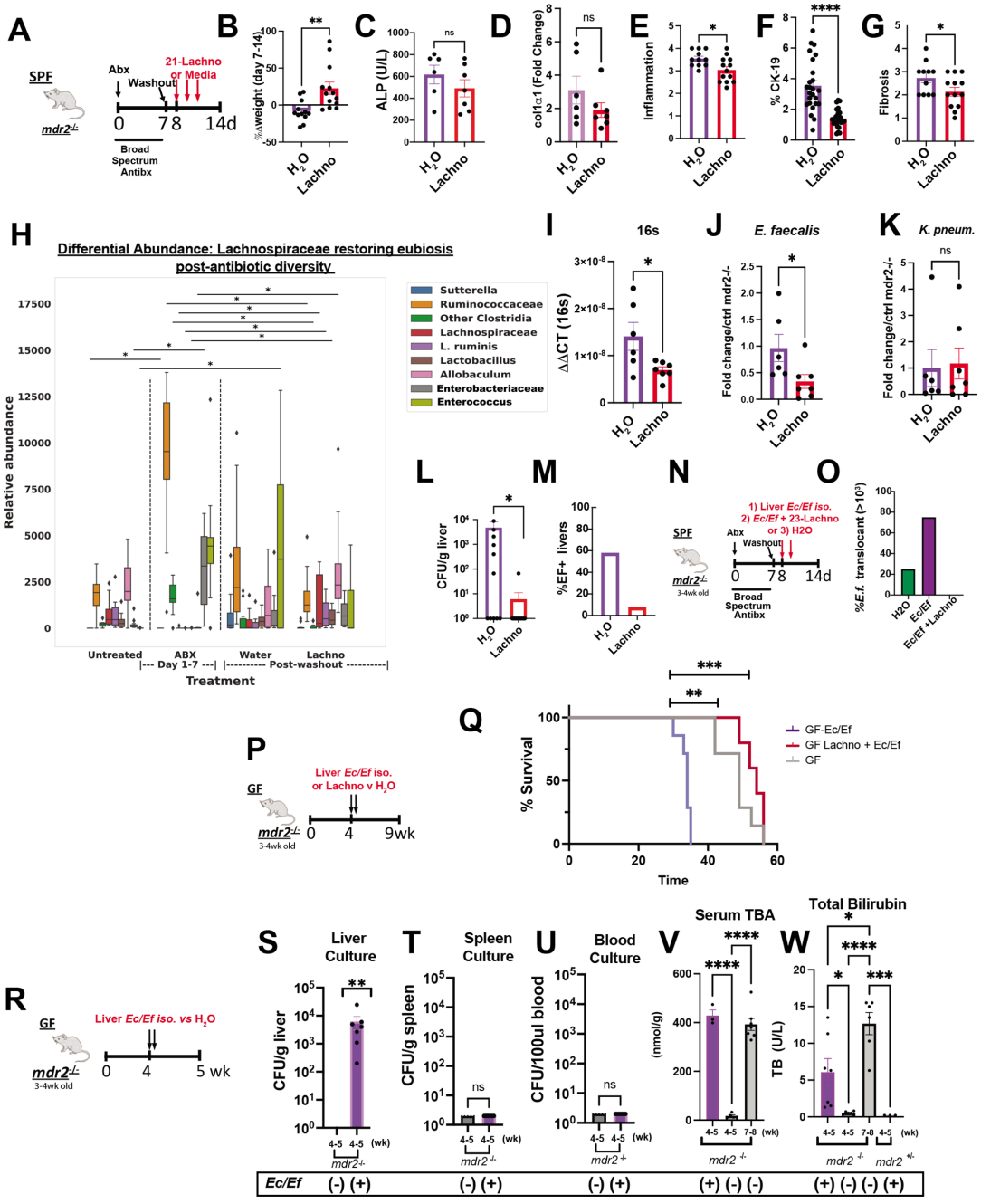

Figure 7 Lachnospiraceae phenotypic and metabolic effects on dysbiosis in *mdr2*$^{-/-}$ mice. Using the 7-day broad-spectrum antibiotic pretreatment model, followed by a 1-day washout, 21 Lachnospiraceae strains (Lachno) versus H_2O were administered to SPF *mdr2*$^{-/-}$ mice on days 8, 10 and 12 (A). Changes following Lachno treatment included Δweight over 7 days (B), serum ALP (C), liver RNA col1α1 expression (D), blinded histological inflammation, ductal reaction and hepatic fibrosis scoring (E–G). Differential abundance expression of 16S rRNA analysis (H) (N, *mdr2*$^{-/-}$ untreated=24, Abx=36, H_2O=11, Lachnospiraceae=13, pooled from two experiments. Presence of universal 16S, Enterococcus and *Klebsiella pneumoniae* (*K. pneum*) faecal DNA by qPCR (I–K) (one of two representative experiment, n=6 mice/group). Hepatic bacterial translocation (L), % of mice with *Enterococcus faecalis* liver translocation (M). Experimental design of treatment of 3–4 week old SPF *mdr2*$^{-/-}$ mice treated with broad-spectrum antibiotic cocktail (vancomycin, neomycin and metronidazole) for 7 days followed by a 1-day washout, then inoculated with *mdr2*$^{-/-}$ resident *Ec/Ef* isolates, versus *Ec/Ef*+23-Lachno combination or water only controls (N) assessing translocated bacteria cultured from homogenised liver (O) (n=4 mice/group). Experiment design (P) and Kaplan-Meyer survival curves (Q) of orally inoculated 10^8 pooled *Ec/Ef* hepatic isolates±Lachnospiraceae (Lachno) or H_2O controls in GF *mdr2*$^{-/-}$mice (H_2O: n=12; *Ec/Ef*: n=7; Lachno: n=6). GF *mdr2*$^{-/-}$ mice were administered 10^8 pooled *Ec/Ef* hepatic isolates and euthanized at 5 weeks in order to measure translocated bacteria to liver, spleen or blood (S–U). Longitudinal measurements of serum TBA and bilirubin conducted in GF *mdr2*$^{-/-}$±*Ec/Ef* hepatic isolates (V and W). Group or pairwise comparisons performed by analysis of variance or Student's t-test, respectively. *P<0.05, **p<0.01, ***p<0.001, ****p<0.0001. GF, germ free; SPF, specific pathogen free.

and Enterococcus (figure 7H). Lachno supplementation resembled the pre-Abx state and particularly repressed Enterococcus expansion versus controls (figure 7H), confirmed by qPCR of faecal samples (figure 7I,J). Lachno treatment did not decrease faecal *Klebsiella pneumoniae*[2] (figure 7K). Importantly, Lachnospiraceae treatment reduced post-ABX culturable hepatic

translocated bacteria (figure 7L). Sanger sequencing identified the translocating strains as *E. faecalis (Ef)* and *E. coli (Ec)*, with *Ef* composing 60% of translocants in Abx-treated SPF *mdr2*$^{-/-}$ mice (figure 7M); all hepatic *Ef* isolates expressed the exotoxin cytolysin (online supplemental figure S3A–D).[25]

Antibiotics increase hepatic translocation of *E. faecalis* and *E. coli*, which accelerate mortality without sepsis

To more directly assess hepatic changes caused by *Ef* and *Ec*, 3–4 week old SPF-antibiotic pretreated or GF *mdr2*$^{-/-}$ mice were colonised with selected *Ec*/*Ef* hepatic isolate strains or H_2O and euthanised at 5 weeks of age (figure 7N). Hepatic translocated *Ec*/*Ef* were isolated in both antibiotic pretreated and gnotobiotic conditions (figure 7O and S) versus untreated controls. Lachno treatment prevented *Ec*/*Ef* liver translocation (figure 5O) and *Ef* faecal concentrations (figure 7J and H). We assessed lethality of these bacteria in gnotobiotic *mdr2*$^{-/-}$ mice by orally inoculating *Ec*/*Ef* isolates with/without Lachno (figure 7P,Q). The *Ec*/*Ef* dual-associated mice exhibited earlier mortality relative to controls (figure 7Q), but survival improved with cocolonisation with Lachno relative to control GF *mdr2*$^{-/-}$ mice. *Ec*/*Ef* isolates colonised GF *mdr2*$^{-/-}$ mice had no evidence of bacteremia or splenic translocation (figure 7T,U). Additionally, *Ec*/*Ef* dual-association accelerated serum BA shunting and associated cholestasis in *mdr2*$^{-/-}$ mice (figure 7V,W). These results demonstrate that *Ec*/*Ef* translocation induces hepatobiliary injury and mortality driven by mechanisms independent of sepsis and systemic bacterial dissemination, and Lachnospiraceae protects from *Ec*/*Ef* hepatic translocation and mortality.

Short-chain fatty acids (SCFAs) produced by Lachnospiraceae have hepatic antifibrogenic effects

We postulate these anti-inflammatory and antifibrotic effects are mediated by Lachnospiraceae metabolic products, including SCFAs that are depleted by selective antibiotics (figure 8b). Vancomycin most effectively decreased SCFA (figure 8b), suggesting vancomycin-sensitive, resident bacteria (like lachnospiraceae) are predominant SCFA producers. Oral supplementation of SCFAs (acetate, propionate and butyrate) in vancomycin-treated *mdr2*$^{-/-}$ mice attenuated hepatic fibrosis (figure 8d–g). The 23 Lachno strains with variable SCFA production were divided into three strains with relatively low (8, 9 and 21-lo) or high (52, 60 and 70-hi) SCFA production as determined by mass spectrometry of supernatants (figure 8h,i). We serially gavaged Hi or Lo SCFA-producing Lachno to SPF *mdr2*$^{-/-}$ mice following antibiotic pretreatment and washout (figure 8i). Hi SCFA-producing Lachno attenuated histological hepatic fibrosis (figure 8j) but not hepatic inflammation (figure 8k) compared with Lo SCFA-producing Lachno. These results provide a mechanism for protection by our Lachnospiraceae consortium.

E. faecalis and Lachnospiraceae are associated with divergent PSC clinical disease activity

Analysis of metagenomic data from multinational repositories (Norway and Germany)[4] of PSC faecal samples identified enrichment of *E. faecalis* and Enterobacteriaceae (figure 9A,B) and depletion of Lachnospiraceae (figure 9C) in PSC patients compared with healthy controls. Both *E. faecalis* (species) and Enterobacteriaceae (family) positively correlated with Mayo risk score (n=51, rho 0.28 for both, p<0.05) in patients with PSC, and Lachnospiraceae Blautia (genus), *Lachnospiraceae bacterium 1_4_56FAA* negatively correlated with Mayo risk score (rho=−0.34 for both, p<0.05) with only a trend at the family level (rho −0.2). *E. faecalis* was more commonly detected in patients with PSC than controls (17% vs 5%) (figure 9D), which was amplified in patients who received antibiotics the last 6 months (figure 9D). Trends existed towards increased Enterobacteriaceae and reduced Lachnospiraceae in patients with antibiotics compared with those without. These clinical results mirror observations in our *mdr2*$^{-/-}$ mice, providing clinical relevance to our murine results.

DISCUSSION

We identified functional subsets of resident luminal bacteria that either potentiate liver inflammation and fibrosis (*E. faecalis* and *E. coli*) or protect (Lachnospiraceae) through distinct mechanisms (figure 7E). We confirmed the overall protection of resident microbiota in GF *mdr2*$^{-/-}$ mice[14 26 27] in a more aggressive genetic background (C57BL/6).[28] We observed early lethality and severe cholestasis in GF *mdr2*$^{-/-}$ mice (median survival: 7.5 weeks) driven by loss of microbial-mediated hepatic accumulation of toxic non-micellular bile salts,[12 29 30] stimulating robust hepatobiliary macrophage recruitment, inflammation, ductular reaction and fibrosis. Supporting progressive hepatic BA accumulation-induced toxic cholangiopathy, ASBTi treatment resulted in faecal BA loss, attenuated serum TBA, improved cholestatic liver and clinical endpoints independent of ileal FGF-15 expression in *mdr2*$^{-/-}$ antibiotic pretreatment model. Early (<5 weeks) but not later (>6 weeks old) autologous SPF FMT rescued this lethal phenotype and cholestasis, validating a strong protective role for SPF *mdr2*$^{-/-}$ microbiota within a short therapeutic window. This brief therapeutic window for effective microbial-mediated protection precludes the likely longer microbial engraftment required to mediate downstream events and mandates intervention at an early inflammatory stage. These preclinical studies imply the need for early-stage clinical microbial therapeutic interventions.

We used broad-spectrum and selective antibiotic treatment to validate protection by host microbiota and, more importantly, to delineate functional therapeutic and detrimental microbial subsets in this model system with shotgun faecal metagenomic and metabolomic analyses. We narrowed the protective microbial community to vancomycin-sensitive populations and metabolites: Lachnospiraceae,[9] Clostridaeceae,[22] BA and SCFA. Selective colonisation of GF and depleted mice with a human Clostridiaceae consortium with protective benefits in colitis models[22] did not confer protection in our model. However, a Lachnospiraceae consortium[24] attenuated hepatic inflammation and fibrosis in antibiotic pretreated mice without changing total faecal BA or FXR/Cyp7a1 signalling, suggesting alternate non-BA mechanisms. Direct supplementation with SCFAsdecreased hepatic fibrogenesis in our vancomycin-Lachnospiraceae depleted SPF model. Antifibrogenic effects of high-SCFA-producing Lachnospiraceae strains suggest that SCFAs partly mediate the protective effects of Lachnospiraceae. Our observations that Lachnospiraceae monoassociation of GF *mdr2*$^{-/-}$ mice decreased hepatic fibrosis but not inflammation or extended lifespan compared with GF mice, yet decreased inflammation, decreased *E. coli* and *E. faecalis* luminal concentrations and hepatic bacterial translocation in antibiotic treateed SPF mice suggest a direct antifibrotic effect of Lachnospiraceae but that their anti-inflammatory benefits are mediated by suppressing resident aggressive species. Metagenomic analysis of feces[4] from a PSC patient cohort demonstrated clinical relevance of our findings and showed decreased Lachnospiraceae species in PSC patients and Lachnospiraceae presence associated with lower Mayo risk scores.

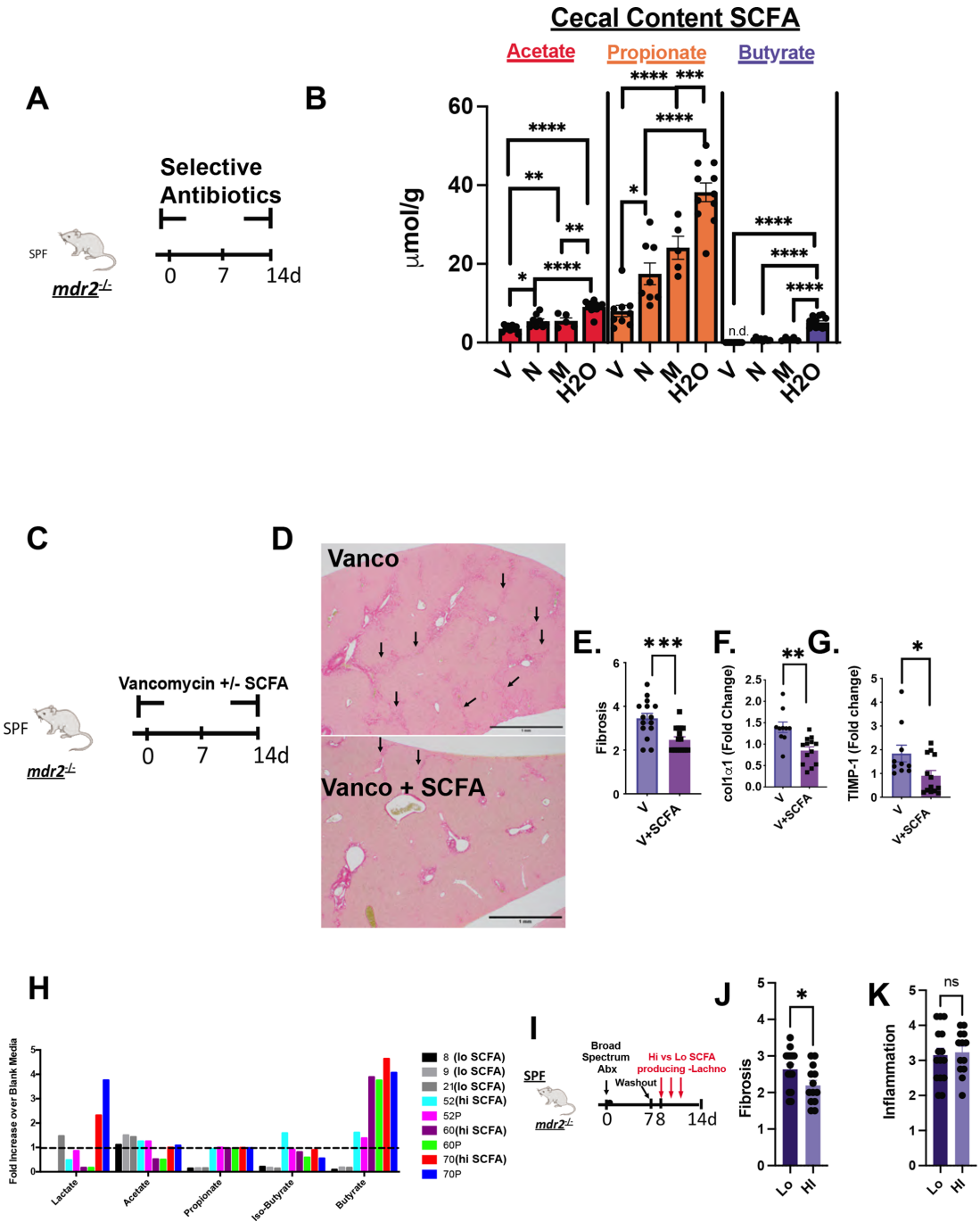

Figure 8 Effect of short-chain fatty acids (SCFAs) on *mdr2*$^{-/-}$ antibiotic model. Experimental design of 14-day selective antibiotic treatment (A) with measurement of cecal content SCFA in SPF *mdr2*$^{-/-}$ mice (B). Design of SPF *mdr2*$^{-/-}$ mice treated with vancomycin (0.5 mg/mL in drinking water, n=10) with or and without SCFA (67.5 mM acetate, 25.9 mM propionate, 40 mM butyrate and 3% sucrose, n=13) ad libitum (C), pooled from two experiments with representative Sirius Red photomicrographs of vancomycin versus vancomycin+SCFA SPF *mdr2*$^{-/-}$ mice, arrows highlight bridging fibrosis (D), blinded histologic fibrosis scoring (E) along with liver RNA col1α1 and *timp1* expression (F–G). Three relatively low and high SCFA-producing (Lo strain #s: 8, 9 and 21; Hi #s: 52, 60 and 70) Lachnospiraceae strains selected from 21 consortium strains were identified by mass spectrometry (H). Experimental design of accelerated antibiotic pretreatment of SPF *mdr2*$^{-/-}$ mice for 7 days and following a 1 day washout, administering Hi or Lo SCFA-producing Lachnospiraceae strains by gavage on days 8, 9 and 10, then followed for 6 days (I) with measurement of histologic hepatic fibrosis (J) and inflammation (K) in Hi compared with Lo SCFA-producing strains. Group or pairwise comparisons performed by analysis of variance or Student's t-test, respectively. *P<0.05, **p<0.01, ***p<0.001, ****p<0.0001.

Other studies show divergent hepatobiliary outcomes of FXR agonism in *mdr2*$^{-/-}$ mice.[14 31] These differences are likely driven by the presence or absence of microbial depletion-mediated expansion of hepatic BA accumulation in each murine model. We found 20× attenuated liver cyp7a1 gene expression and increased hepatic BA accumulation in GF compared with SPF *mdr2*$^{-/-}$ mice, despite no difference in ileal FGF15 expression (a key downstream FXR target). Despite increased total serum BA, no difference in ileal FGF-15 expression was similarly reported recently by Schneider *et al*[14] between antibiotic treated

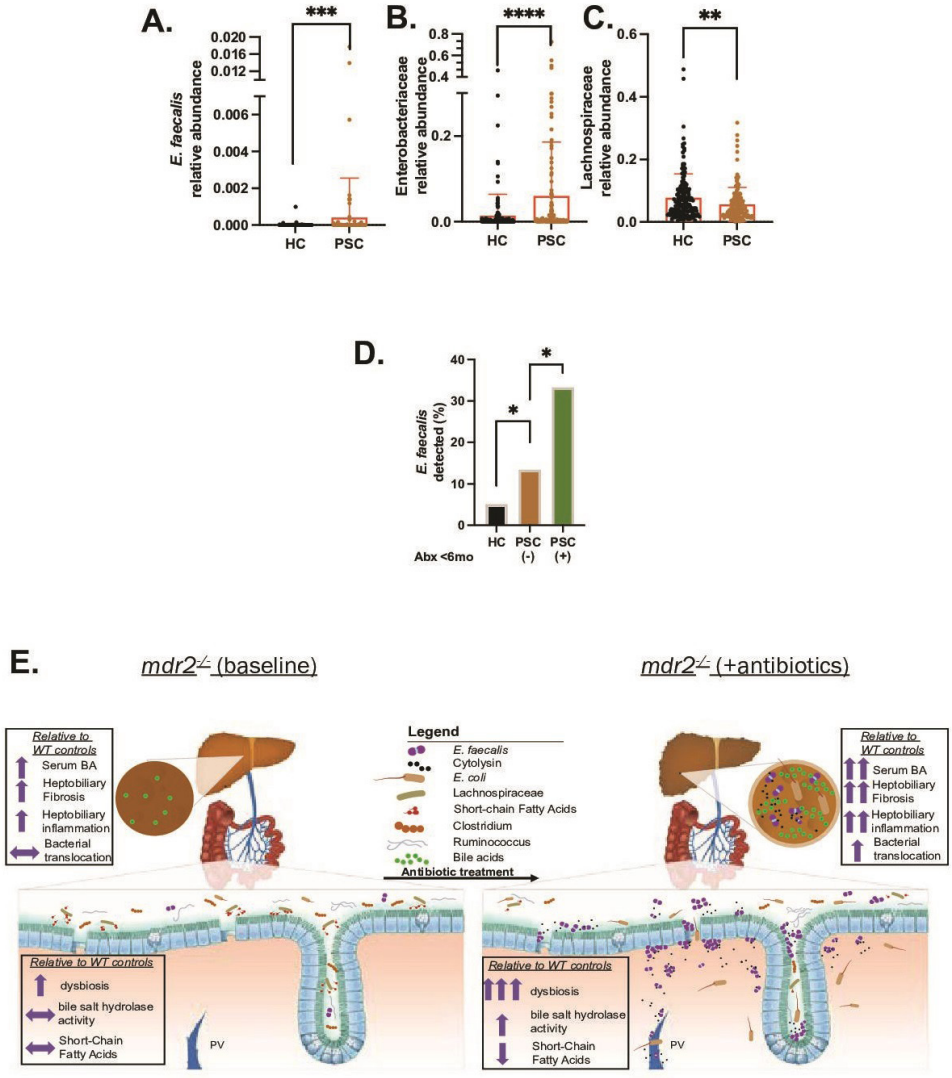

Figure 9 Selective faecal bacterial profile in PSC patients and effect of antibiotic exposure. Relative abundance of faecal *Enterococcus faecalis* (*E. faecalis*) (A), Enterobacteriaceae (B) and Lachnospiraceae (C) in heathy controls (HCs; n=158) versus PSC patients (n=136). (D) Prevalence of faecal *E. faecalis* in HC (irrespective of antibiotics use) versus PSC patients exposed to antibiotics (n=24) and no antibiotics exposure (n=112) the last 6 months. Data in figure parts A–C compared with Mann–Whitney U test, (D) with Fisher's exact test. Graphical summary depicting the effect of antibiotic-induced dysbiosis of SPF *mdr2*$^{-/-}$ mice to potentiate hepatobiliary disease with hepatic translocation of *E. faecalis* and *Escherichia coli*, increased bile salt hydrolase activity (conjugated/unconjugated BA), hepatic bile acid pool size, and decreased SCFA production (E). *P<0.05, **p<0.01, ***p<0.001, ****p<0.0001. BA, bile acid; PSC, primary sclerosing cholangitis; SCFA, short-chain fatty acid.

vs untreated *mdr2*$^{-/-}$ mice, suggesting a microbial based, FXR-independent driver of hepatic BA accumulation in this model.[12]

We demonstrated clinical evidence of positive and negative correlations with Mayo risk score between both resident pathobionts (*E. faecalis* and Enterobacteriaceae) and protective Lachnospiraceae, respectively. In addition, *E. faecalis* expand in PSC patients exposed to antibiotics. Unfortunately, the antibiotic type and spectrum were unavailable in our clinical data set. Vancomycin clinical studies show heterogenous biochemical responses in PSC patients,[32] suggesting individual vancomycin therapeutic effects on protective and pathogenic bacteria. These studies lack baseline and postintervention microbial profile assessments necessary to assess antibiotic microbial targets. Our *mdr2*$^{-/-}$ results suggest that broad-spectrum antibiotics should be administered with caution in PSC patients due to potential for exacerbating disease and contributing to recurrent cholangitis by promoting enterohepatic bacterial translocation.

This study has several limitations. Early lethality of our GF and broad-spectrum antibiotic-depletion *mdr2*$^{-/-}$ mice precluded longitudinal studies to assess delayed effects of Lachnospiraceae or SCFA on chronic disease progression. Second, we acknowledge the ongoing controversy regarding suitability of murine AP to monitor cholestasis.[33 34] Therefore, we confirmed our findings with TB and bile duct reactivity as additional markers of cholestatic injury. Finally, because GF *mdr2*$^{-/-}$ mice expire before becoming fertile, our heterozygous *mdr*$^{+/-}$ breeding strategy with small litter sizes delayed experiments and limited more ± depth mechanistic studies but permitted littermate control comparisons.

Our mechanistic studies have direct translational implications for future personalised bacterial manipulation in PSC patients. For example, carefully screened cohorts of PSC patients may optimally respond to selective depletion of disease-inducing subsets and/or augmentation of protective bacteria or secreted metabolites. Additionally, our gnotobiotic model can explore hepatobiliary, microbial

and metabolomic impacts of humanised faecal transfer and selective colonisation with WT and genetically engineered bacterial strains to dissect microbial protective and pathogenic mechanisms. This study also highlights specific in vivo roles for bacteria, such as Lachnospiraceae, play require additional protective resident bacteria to recapitulate various protective effects transferred by faecal microbiota transplantation. Future directions will determine the influence of macrophage phenotypes,[35] downstream SCFA targets and activities of other putative protective bacteria on experimental hepatobiliary inflammation and fibrosis. In conclusion, our gnotobiotic and antibiotic *mdr2*$^{-/-}$ PSC murine models identified complex interactions between novel hepatoprotective resident bacteria balanced against pathobionts, replicated in PSC patient cohorts. Resident bacterial subsets exert both positive and negative influences partly through antimicrobial activities and altering bacterial metabolites.

Author affiliations
[1]Division of Gastroenterology and Hepatology, University of North Carolina System, Chapel Hill, North Carolina, USA
[2]Center for Gastrointestinal Biology and Disease, University of North Carolina System, Chapel Hill, North Carolina, USA
[3]Department of Genetics, University of North Carolina System, Chapel Hill, North Carolina, USA
[4]Department of Gastroenterology, Indiana University School of Medicine, Indianapolis, Indiana, USA
[5]Department of Microbiology and Immunology, University of North Carolina System, Chapel Hill, North Carolina, USA
[6]Department of Environmental Sciences and Engineering, Gillings School of Global School of Public Health, University of North Carolina System, Chapel Hill, North Carolina, USA
[7]Department of Pathology, Division of Comparative Medicine, and Lineberger Comprehensive Cancer Center, University of North Carolina System, Chapel Hill, North Carolina, USA
[8]Norwegian PSC Research Center, Oslo University Hospital, Rikshospitalet, Oslo, Norway
[9]Institute of Clinical Medicine, University of Oslo, Oslo, Norway
[10]Institute of Clinical Molecular Biology, Zentrums für Molekulare Biowissenschaften, Kiel, Schleswig-Holstein, Germany
[11]University Medical Centre Hamburg-Eppendorf, Hamburg, Germany
[12]Institute of Clinical Molecular Biology, Christian-Albrechts-University of Kiel, Kiel, Germany
[13]Department of Environmental Sciences and Engineering, University of North Carolina at Chapel Hill, Chapel Hill, North Carolina, USA
[14]Department of Microbiology and Immunology, Virginia Commonwealth University School of Medicine, Richmond, Virginia, USA
[15]Department of Research, McGuire Veterans Affairs Medical Cente, Richmond, Virginia, USA
[16]Virginia Commonwealth University Medical Center, Richmond, Virginia, USA
[17]UNC Lineberger Comprehensive Cancer Center, Center for Translational Immunology, University of North Carolina, Chapel Hill, Chapel Hill, North Carolina, USA
[18]Department of Gastroenterology, Beth Israel Deaconess Medical Center/Harvard Medical School, Boston, Massachusetts, USA
[19]Norwegian PSC Research Center, Department of Transplantation Medicine, Oslo University Hospital, Oslo, Norway
[20]Indiana University School of Medicine, Indianapolis, Indiana, USA
[21]Richard L. Roudebush VA Medical Center, Indianapolis, Indiana, USA

Twitter Johannes Roksund Hov @hov_jer

Acknowledgements Bo Liu, DVM, PhD, and Akihiko Oka, MD, PhD, provided technical assistance; Josh Frost, UNC Gnotobiotic Facility Manager for gnotobiotic research support; Fengling Li, MD, PhD, and Allison Rogala, DVM, for germ-free derivation of *mdr2*$^{-/-}$ mice; Lisa Holt for laboratory management and Cary Cotton for statistical support. Special appreciation to Dr Vincent Young, University of Michigan, for providing the original Lachnospiraceae stains and to Dr Kenya Honda, Rikken Institute, Tokyo, for providing the Clostridium consortium species. Special thanks to UNC Clinical Chemistry and CGIBD Pathology Cores for assistance with liver enzyme analysis and histologic preparation and staining.

Contributors MA and RBS are guarantors of the paper. MA and RBS conceptualised the study. MA, BN, AV and MF contributed to the collection of samples. JT and JPYT grew and contributed Lachnospiraceae strains. KL and YL were responsible for metabolomics. JW performed the postsequencing data processing. SM performed blinded H&E and Sirius Red histological scoring. VM and HLF performed IHC staining along with image analysis. HZ, PBH, JSB and MA performed bile acid analysis. MA executed statistical analysis and data organization. MK, LT, SC, CB, AF and JRH collected and analysed human faecal metagenomic data. MA, VM, JW, JT, MK, YL, KL, JPYT, HLF and RBS performed data curation. YVP provided murine resources and technical advice. MA, JW and RBS planned the analysis reviewed data and edited the results. MA, JW, MK, JRH and RBS performed formal analysis. MA and RBS interpreted data. RBS supervised the study, and MA was responsible for project administration. MA and RBS wrote the original draft. MA, JW and RBS contributed to the writing of the manuscript. All authors read, critically revised for important intellectual content, and approved the final manuscript. RBS and MA acquired funding.

Funding National Institute Health (NIH) grants P01DK094779, P40OD10995 and P30DK034987 (to RBS), K01DK119582 (to JW); T32DK07737 and T322A1007273 (to MA), The Crohn's and Colitis Foundation #2434 (to RBS); CA232109, DK094779 and AI067798 (to JT); VA 1I01BX003031 and IK6BX005226; DK108959 and DK119421 (to HLF). JRH is funded by the European Research Council, grant no. 802544. CS is supported by the DFG, CRU306, and by the Helmut and Hannelore Greve Foundation and grant support from BiomX and Galapagos. VA Merit Award I01BX004033; Research Career Scientist Award (IK6BX004477); VA ShEEP Grant (1 IS1 BX004777); NIH Grants R01 DK104893, R01DK-057543 (to HZ). VA Merit Review 2I0CX001076, R21TR003095 (NCATS) (to JSB). VA Merit Award BX001328 (to PBH).

Competing interests RBS has consulted for and received grant support from Takeda, Janssen, Second Genome, Vedanta, BiomX, Biomica, SERES and Artizan; JRH has served on advisory boards and/or given lectures for Orkla Health, Novartis, Amgen and Roche, and received research support from Biogen, all unrelated to the present study.

Patient and public involvement Patients and/or the public were not involved in the design, or conduct, or reporting, or dissemination plans of this research.

Patient consent for publication Consent obtained directly from patient(s)

Ethics approval Ethical approval was obtained from the respective Local Ethics Committees (Norway: Regional Committee for Medical and Health Research Ethics in South-Eastern Norway (reference number 2015/2140); Germany: Hamburg (reference number MC-111/15) and Kiel (reference numbers A148/14, A117-13 and A156-03)). We conducted mouse studies under the NIH guide for Care and Use of Laboratory Animals, approved and overseen by the UNC-Chapel Hill Institutional Animal Care and Use Committee (Protocol ID 18–266). Participants gave informed consent to participate in the study before taking part.

Provenance and peer review Not commissioned; externally peer reviewed.

Data availability statement Data are available on reasonable request. All data relevant to the study are included in the article or uploaded as supplementary information.

ORCID iDs
Muyiwa Awoniyi http://orcid.org/0000-0002-5811-070X
Martin Kummen http://orcid.org/0000-0001-9660-6290
Corinna Bang http://orcid.org/0000-0001-6814-6151
Huiping Zhou http://orcid.org/0000-0002-0050-372X
Yury V Popov http://orcid.org/0000-0001-7973-942X
Johannes Roksund Hov http://orcid.org/0000-0002-5900-8096
Ryan Balfour Sartor http://orcid.org/0000-0002-7820-632X

REFERENCES

1 Weismüller TJ, Trivedi PJ, Bergquist A, *et al*. Patient age, sex, and inflammatory bowel disease phenotype associate with course of primary sclerosing cholangitis. *Gastroenterology* 2017;152:e8:1975–84.

2 Nakamoto N, Sasaki N, Aoki R, *et al*. Gut pathobionts underlie intestinal barrier dysfunction and liver T helper 17 cell immune response in primary sclerosing cholangitis. *Nat Microbiol* 2019;4:492–503.
3 Liwinski T, Zenouzi R, John C, *et al*. Alterations of the bile microbiome in primary sclerosing cholangitis. *Gut* 2020;69:665–72.
4 Kummen M, Thingholm LB, Rühlemann MC, *et al*. Altered gut microbial metabolism of essential nutrients in primary sclerosing cholangitis. *Gastroenterology* 2021;160:1784–98.
5 Kunzmann LK, Schoknecht T, Poch T, *et al*. Monocytes as potential mediators of pathogen-induced T-helper 17 differentiation in patients with primary sclerosing cholangitis (PSC). *Hepatology* 2020;72:1310–26.
6 Tedesco D, Thapa M, Chin CY, *et al*. Alterations in intestinal microbiota lead to production of interleukin 17 by intrahepatic γδ T-cell receptor-positive cells and pathogenesis of cholestatic liver disease. *Gastroenterology* 2018;154:2178–93.
7 Katt J, Schwinge D, Schoknecht T, *et al*. Increased T helper type 17 response to pathogen stimulation in patients with primary sclerosing cholangitis. *Hepatology* 2013;58:1084–93.
8 Torres J, Palmela C, Brito H, *et al*. The gut microbiota, bile acids and their correlation in primary sclerosing cholangitis associated with inflammatory bowel disease. *United European Gastroenterol J* 2018;6:112–22.
9 Truax AD, Chen L, Tam JW, *et al*. The inhibitory innate immune sensor NLRP12 maintains a threshold against obesity by regulating gut microbiota homeostasis. *Cell Host Microbe* 2018;24:364–78.
10 Vleggaar FP, Monkelbaan JF, van Erpecum KJ. Probiotics in primary sclerosing cholangitis: a randomized placebo-controlled crossover pilot study. *Eur J Gastroenterol Hepatol* 2008;20:688–92.
11 Allegretti JR, Kassam Z, Carrellas M, *et al*. Fecal microbiota transplantation in patients with primary sclerosing cholangitis: a pilot clinical trial. *Am J Gastroenterol* 2019;114:1071–9.
12 Out C, Patankar JV, Doktorova M, *et al*. Gut microbiota inhibit Asbt-dependent intestinal bile acid reabsorption via GATA4. *J Hepatol* 2015;63:697–704.
13 Wang R, Sheps JA, Liu L, *et al*. Hydrophilic bile acids prevent liver damage caused by lack of biliary phospholipid in *Mdr2*$^{-/-}$ mice. *J Lipid Res* 2019;60:85–97.
14 Schneider KM, Candels LS, Hov JR, *et al*. Gut microbiota depletion exacerbates cholestatic liver injury via loss of FXR signalling. *Nat Metab* 2021;3:1228–41.
15 Fickert P, Fuchsbichler A, Wagner M, *et al*. Regurgitation of bile acids from leaky bile ducts causes sclerosing cholangitis in Mdr2 (Abcb4) knockout mice. *Gastroenterology* 2004;127:261–74.
16 Franz CM, Specht I, Haberer P, *et al*. Bile salt hydrolase activity of enterococci isolated from food: screening and quantitative determination. *J Food Prot* 2001;64:725–9.
17 Chand D, Panigrahi P, Varshney N, *et al*. Structure and function of a highly active bile salt hydrolase (BSH) from Enterococcus faecalis and post-translational processing of BSH enzymes. *Biochim Biophys Acta Proteins Proteom* 2018;1866:507–18.
18 Ikenaga N, Liu SB, Sverdlov DY, *et al*. A new Mdr2(-/-) mouse model of sclerosing cholangitis with rapid fibrosis progression, early-onset portal hypertension, and liver cancer. *Am J Pathol* 2015;185:325–34.
19 Hoentjen F, Harmsen HJM, Braat H, *et al*. Antibiotics with a selective aerobic or anaerobic spectrum have different therapeutic activities in various regions of the colon in interleukin 10 gene deficient mice. *Gut* 2003;52:1721–7.
20 Madsen KL, Doyle JS, Tavernini MM, *et al*. Antibiotic therapy attenuates colitis in interleukin 10 gene-deficient mice. *Gastroenterology* 2000;118:1094–105.
21 Ghallab A, Hofmann U, Sezgin S, *et al*. Bile microinfarcts in cholestasis are initiated by rupture of the apical hepatocyte membrane and cause shunting of bile to sinusoidal blood. *Hepatology* 2019;69:666–83.
22 Atarashi K, Tanoue T, Oshima K, *et al*. Treg induction by a rationally selected mixture of clostridia strains from the human microbiota. *Nature* 2013;500:232–6.
23 Frank DN, St Amand AL, Feldman RA, *et al*. Molecular-phylogenetic characterization of microbial community imbalances in human inflammatory bowel diseases. *Proc Natl Acad Sci U S A* 2007;104:13780–5.
24 Chen L, Wilson JE, Koenigsknecht MJ, *et al*. NLRP12 attenuates colon inflammation by maintaining colonic microbial diversity and promoting protective commensal bacterial growth. *Nat Immunol* 2017;18:541–51.
25 Duan Y, Llorente C, Lang S, *et al*. Bacteriophage targeting of gut bacterium attenuates alcoholic liver disease. *Nature* 2019;575:505–11.
26 Tabibian JH, O'Hara SP, Trussoni CE, *et al*. Absence of the intestinal microbiota exacerbates hepatobiliary disease in a murine model of primary sclerosing cholangitis. *Hepatology* 2016;63:185–96.
27 Mazagova M, Wang L, Anfora AT, *et al*. Commensal microbiota is hepatoprotective and prevents liver fibrosis in mice. *Faseb J* 2015;29:1043–55.
28 Peng Z-W, Rothweiler S, Wei G, *et al*. The ectonucleotidase ENTPD1/CD39 limits biliary injury and fibrosis in mouse models of sclerosing cholangitis. *Hepatol Commun* 2017;1:957–72.
29 Ikeda Y, Morita S-Y, Terada T. Cholesterol attenuates cytoprotective effects of phosphatidylcholine against bile salts. *Sci Rep* 2017;7:306.
30 Smit JJ, Schinkel AH, Oude Elferink RP, *et al*. Homozygous disruption of the murine mdr2 P-glycoprotein gene leads to a complete absence of phospholipid from bile and to liver disease. *Cell* 1993;75:451–62.
31 Baghdasaryan A, Claudel T, Gumhold J, *et al*. Dual farnesoid X receptor/TGR5 agonist INT-767 reduces liver injury in the Mdr2-/- (Abcb4-/-) mouse cholangiopathy model by promoting biliary HCO^{-}_{3} output. *Hepatology* 2011;54:1303–12.
32 Shah A, Crawford D, Burger D, *et al*. Effects of antibiotic therapy in primary sclerosing cholangitis with and without inflammatory bowel disease: a systematic review and meta-analysis. *Semin Liver Dis* 2019;39:432–41.
33 Krones E, Erwa W, Trauner M, *et al*. Serum alkaline phosphatase levels accurately reflect cholestasis in mice. *Hepatology* 2015;62:981–3.
34 Halling Linder C, Englund UH, Narisawa S, *et al*. Isozyme profile and tissue-origin of alkaline phosphatases in mouse serum. *Bone* 2013;53:399–408.
35 Guicciardi ME, Trussoni CE, Krishnan A, *et al*. Macrophages contribute to the pathogenesis of sclerosing cholangitis in mice. *J Hepatol* 2018;69:676–86.

Supplemental Material and Methods:

Liver Histology and Immunohistochemistry Analysis:

H&E, Sirius red and trichrome-stained liver sections were scored by a board-certified veterinary pathologist blinded to experimental groups who assessed fibrosis and periportal/biliary inflammation in a minimum of 12 portal systems within at least two liver lobes. Fibrosis was scored by modified Ludwig criteria [36]: 0, no fibrosis; 1, focal portal/periportal fibrosis, minimal extension into septa; 2, multifocal fibrosis, most (>50%) of portal areas displaying septal fibrosis; 3, fibrosis with most (≥ 50%) portal areas expanded with occasional portal-portal bridging; 4, expanded portal areas with marked (>50%) portal-portal or portal-central bridging; 5, marked bridging with occasional nodules (incomplete cirrhosis); 6, multilobular nodular fibrosis. Periportal/biliary inflammation (0-5) scoring: 0, no inflammation; 1, increased individual inflammatory cells, with rare, loose aggregates (<3 cells); 2, inflammatory cells piling up ≥3 cells deep, +/- rare individual cells in the biliary epithelium; 3, greater aggregation of inflammatory cells expanding/infiltrating along the limiting plate (but not fully connecting to adjacent portal triad) +/- early focal disruption of parenchymal or ductal architecture; 4, more severe than 3, with multifocal single duct architectural disruption, focal areas with more severe architectural disruption along the entire limiting plate between two adjacent portal systems, +/- inflammation with hepatobiliary cell death; 5, severe portal inflammatory infiltrate (loss of lobular architecture with >50% parenchymal inflammatory cell disruption), inflammatory periportal involvement extending to zone 3. We measured hepatic ductular reaction by CK-19, macrophages by F4/80, and neutrophils by MPO staining performed by immunohistochemistry and

semiquantification analysis with Image Pro (Media Cybernetics Inc., Rockville, MD) as previously described. [37,38] Briefly, liver sections (4μm thickness) were deparaffinized and antigen epitope was unmasked with citrate-based heat antigen retrieval following manufacturers protocol (Vector Laboratories, Burlingame, CA). Endogenous peroxidase activity was blocked with hydrogen peroxide and non-specific binding was blocked with 5% BSA prior to overnight incubation with primary antibody at 4°C. Secondary antibody was incubated for 1 hour at room temperature and positive staining was detected via 3,3′-Diaminobenzidine (DAB) following the manufacturer's protocol (Vector Laboratories, Burlingame, CA). Modified Harris hematoxylin provided regressive counterstaining for general nuclear and cytoplasmic staining. Slides were imaged at 100X or 200X magnification with three to five representative sections per mouse with ImageScope 12.1 (Leica, Wetzlar, Germany).

Permeability studies in vivo:

We have optimized FITC-dextran (44kDa, Sigma Aldrich in vivo permeability for distal small intestine/colon (verified by Wood's lamp). Mice were fasted overnight followed by oral gavage of FITC-dextran. Serum collected and read on read on a CLARIOstar Plate Reader (BMG LABTECH in Offenburg, Germany).

Assessing of Bacterial Liver Translocation:

Left lobe (40mg) was sterilely homogenized in 200ml of PBS. 100ml was plated and serially diluted homogenously and spread onto UTI ChromoSelect Agar (Millipore/Sigma 16636) after initially plating on non-selective BHI plates. Colonies were counted after overnight incubation (37ºC). Red-pink and blue colonies representing *E. coli* and

Enterococcus spp (β-D-galactosidase and ß-glucosidase enzyme activity, respectively), were counted and multiplied by the dilution factor. Sanger sequencing verified colonies as *E. faecalis* or *E. coli*.

Primary Sclerosing Cholangitis (PSC) Patient Fecal Analysis:

We analyzed shotgun metagenomic data of fecal samples from 136 patients with PSC and 158 healthy controls. PSC antibiotic (Abx) exposure was defined between 6 weeks and 6 months before study inclusion (+Abx=24, no Abx=112), Abx users within 6 weeks before study inclusion were excluded. Processing and biostatistical analysis were as described.[4]

Bile Acid Analysis:

Serum TBA concentration was determined using the Diazyme Total BA Universal (Diazyme Laboratories, Poway, CA, (DZ042-A-K01)) read on a CLARIOstar Plate Reader (BMG LABTECH in Offenburg, Germany).

Fecal and liver bile acid underwent methanol and acetonitrile tissue processing and isolation prior to injection for LC-MS/MS analysis (conducted by the Zhou laboratory at Virginia Commonwealth University). Quantification using standard a combination of deuterium-labeled and unlabeled internal standards. LC–MS/MS analysis was carried out using a Shimadzu CBM-20A CL communications bus module. The MS analysis was done using an LCMS-8060 CL triple quadrupole instrument with an electrospray ionization source (Shimadzu, Japan). Data acquisition and analysis was performed by

Labsolutions insight.The 7α-hydroxy-4-cholesten-3-one (C4) assay performed by the Zhou laboratory based on HPLC/tandem mass spectrometry. HPLC-MS/MS for bile acid compounds and C4 was optimized in the ESI negative and positive modes, respectively. The total BA (TBA) value is calculated by summing the values of all evaluated BA forms.

ASBT inhibition assay

GSK23306(Linerixibat, a specific ASBT inhibitor) was synthesized by Cayman chemical (23843, Ann Arbor, MI). Three-four week old *mdr2*$^{-/-}$ mice undergoing accelerated 7-day antibiotic pretreatment protocol with GSK23306 (10mg/kg in sterile H_2O) or no GSK23306 for 2 weeks animal weight, BA, molecular and histological data analysis were conducted with tissue samples at time of euthanasia.

Bacterial inoculation/fecal transplant experiments and SCFA administration:

mdr2$^{-/-}$ mouse liver-derived *E. fecalis* and *E. coli,* 17-strain Clostridia (Atarashi Nature 2013), human *E. fecalis* cytolysin active/inactive strains (gift from Dr. Schnable lab), & 23-strain *Lachnospiraceae*[23] were orally gavaged with 10^8 CFU of bacteria/200ul sterile PBS in combination or alone in antibiotic-treated or GF *mdr2*$^{-/-}$ and littermate controls. Bacterial culture media consisted of brain-heart infusion broth (BHI) supplemented with 5% FBS, 0.01% L-cysteine and 1% corn starch twice a week for 2-4 weeks before harvest. Plain BHI medium was used as the vehicle control. Mice were inoculated twice weekly for 2 weeks. For antibiotic SCFA experiments, SPF MDR2-/- mice exposed to *ad libitum* drinking of mixture of vancomycin, (1mg/ml) alone or with SCFA cocktail of 67.5

mM acetate, 40 mM butyrate, 25.9 mM propionate (Sigma-Aldrich) were given to mice in DI H20 [36].

For fecal contents transplant experiments, we transplanted feces collected from SPF *mdr2*$^{-/-}$ C57BL/6 mice diluted in PBS at a ratio of 100mg of pre-reduced anaerobic feces/ml that was homogenized in a bead beater. The insoluble particles were removed by passing the mixture through a laboratory stainless sieve. Total bacterial protein concentration was determined by BCA assay to normalize the amount of bacterial cells. The feces mixtures were stored in -80C until needed for use. We orally gavaged with 200ul of fecal mixture twice every 3 days during the first week.

E.faecalis Gelatinase and Cytolysin Agar Assays:

We performed an adapted cytolysin hemolytic assay from previous studies [37] to identify *E.faecalis* cytolysin activity. Human Gilmore *E. Faecalis* cytolysin active and inactive strains [24] (kind gift from Dr. Schnabl laboratory) were compared to isolated *mdr2*$^{-/-}$ liver colonized *E.fecalis* and *E.coli* strains from 8 different mice following antibiotic administration and plated on sheep blood agar plates (BD BBL Agar) incubated overnight at 37°C. Twenty-four hour plates were assessed for -b-hemolytic activity compared to control strains (S5F).

E. faecalis V583 (originally isolated from infected human blood) and DgelE isogenic mutant was generated as described previously [38]and a kind gift from Dr. Carroll's laboratory was used in our study for positive and negative gelatinase activity controls. The abilities of *E. faecalis* V583 and DgelE isogenic mutant to degrade casein were tested using BHI agar containing 2.5% skim milk with a methodology similar to that of

previously described work[38] compared to isolated *mdr2*$^{-/-}$ liver colonized *E.fecalis* strains from 8 different mice following antibiotic administration (S5E). Additionally, 30ul (1e8/ml) aforementioned bacterial group suspensions were placed in a linear line onto skim milk agar plates and was incubated overnight at 37°C. A zone of clearing surrounding E. faecalis cells indicated caseinolytic/gelatinase activity (S5G).

Biochemical Assessment of Fibrosis:

Hydroxyproline (HYP) was determined biochemically as previously described [39]. Briefly, two snap-frozen liver pieces from the left and right liver lobe (100-150 mg additive total) were hydrolyzed in 5 ml 6 N HCl at 110C for 16 h. Based on relative hepatic HYP (per 100 mg of wet liver), total hepatic HYP were calculated (per total liver, as obtained by multiplying liver weights with relative hepatic HYP).

Real-time qPCR:

Consistent snap frozen right hepatic lobes were stored in RNAlater (Thermo Fisher) at -80C. A small proportion was removed from storage solution and homogenized and total RNA isolation via RNeasay Mini Kit (QIAGEN) according to the manufacturer's recommendations. cDNA was obtained by reverse transcription of 250ng of total RNA using iScript cDNA Synthesis Kit (Biorad) according to the instructions of the manufacturer. Relative mRNA transcript levels were quantified using TaqMan Universal PCR Master Mix (Applied Biosystems) applying the TaqMan methodology or iTaq Universal SYBR Green Supermix (Biorad) for SYBR green probes (3.75 pmol of each primer and an estimated 6.25ng of

complementary DNA (cDNA) were set up with each sample in duplicate-triplicates on 96-well plates (Sarstedt, Numbrecht, Germany). The housekeeping gene 18s was amplified in a parallel reaction for normalization. Primers for the following genes were used: Monocyte Chemoattractant Protein-1 (MCP-1), Lipocalin-2 (Lcn-2), Collagen 1a1 (Col1a1), Tissue inhibitor of metalloproteinases (Timp)-1, inducible nitric oxide (iNos)-2, Interleukin-(IL)-6, Tumor Necrosis Factor (TNF)-alpha. Primer sequences are detailed summarized in Table S2. All TaqMan probes are positioned on exon–exon boundaries of corresponding genes to exclude co-amplification of genomic DNA. Sense and antisense primer (each at 0.5 mM) and 0.125 mM50-phoshorylated probe, labeled at its 50-end with the reporter dye 6-carboxyfluorescein (6-FAMe) and at the 30end with the quencher dye 6-carboxy-tetramethyl-rhodamine (TAMRA), were synthesized by ThermoFisher. The relative expression of each sample was first normalized to the expression of the reference gene 18s, and then normalised to the average expression in samples from *mdr2*$^{-/-}$ mice, and the data were analysed according to the 2^{-DDCT} method.

Serum collection

Blood was collected by cardiac puncture at the time of mouse necropsy, and serum was separated using BD serum separator additive microtainer tubes and centrifugation at 4000 x g rcf for 15 minutes. The recovered serum was stored at -80ºC.

Liver Function Tests:

Serum from fresh blood was made by using BD Microtainer SST tubes (Ref: 365967), and saved in -20C in less than a week before measurement in Clinical Chemistry Core of University of North Carolina in Chapel Hill. Each chemistry test was calibrated and

QCed right before measuring using GEMCAL reference serum(S1-33) and LEVEL1 Chemistry Control(Ref: C1-4) and Level 2 Chemistry Control(Ref:C1-5). They are all from Alfawassermann Diagnostic Technologies, LLC.The serum levels of ALT, ALP, Tbil were measured using the kits of ALT, ALP, and Tbil from Alfawassermann with references of SA1052, SA2002, and SA1008, respectively.

Bacterial DNA Isolation/16s rRNA Sequencing/ Analysis Methods:

Fecal samples were collected from live mice, snap-frozen and stored at -80C. DNA was isolated by incubating fecal material at 65^{o} C for 30min in Lysing Matrix E tubes (MP Biomedicals) containing 200mM NaCl, 100mM Tris, 20mM EDTA (pH 8.0), SDS and proteinase K (QIAGEN). Phenol:Chloroform:Isoamyl alcohol (25:24:1) (Invitrogen) was added, and the samples were homogenized at 4C for 3min using a bead beater homogenizer. The samples were centrifuged at 8000 rpm for 3min at 4C, and the supernatant was incubated with equal volume of Phenol:Chloroform:Isoamyl alcohol for 10 min at room temperature. The samples were centrifuged at 13,000rpms for 5min at 4^{o} C, and the aqueous phase was incubated with isopropanol and 3M sodium acetate, pH 5.2, at -20^{o} C for 15hrs to precipitate DNA. The precipitated DNA was collected by centrifugation at 13,000rpm at 4^{o} C for 20min, washed twice with 100% cold ethanol and resuspended in TE buffer. The DNA was further purified using a DNeasy Blood and Tissue Kit (QIAGEN) according to the manufacturer's protocol.

Fecal DNA samples were amplified by PCR and amplified the 16S V4 hypervariable region using 515F and 806R universal primers. We multiplexed (128/120) samples using 12 nt golay barcodes and were sequenced on an Illumina MiSeq to produce (27/67) million paired-end 250bp reads for a total of (6.9/16.7) Gbp. Primers and

barcodes were trimmed from reads to an average of 220bp. Exp1 had a minimum of 8,291 reads per sample with an average of 71,369. Exp2 had a minimum of 37,544 reads/sample and an average of 154,578 reads/sample.

We used the DADA2 module in QIIME2 to merge, denoise, and produce amplicon sequence variants (ASVs). ASVs were assigned to representative taxa with the QIIME2 tool classify-sklearn using the Greengenes database (gg-13-8). All alpha and beta diversity, differential abundance, PCoA, and group significance analyses were performed using the respective QIIME2 tools. Phylogenetic diversity was computed for ASVs by aligning sequences with MAFFT and building a phylogenetic tree with FastTree. Differential abundance was computed among taxa collapsed at several taxonomic levels using ANCOM, corrected for multiple testing using the Holm-Bonferroni method. Functional predictions to the KEGG ontology were made using the PICRUSt 2 custom tree pipeline in QIIME2.

Metabolomic Analysis:

All analyses of metabolites in serum and cecal content were performed at UNC Chemistry and Analytic Core. A UHPLC/Q-TOF method was used for metabolomic analysis of both serum and cecal content samples. The system consisted of an Agilent 1290 Infinity II LC system (Agilent Technologies, Santa Clara, CA) with a pump (G7120A), a column chamber (G7116B), a multisampler (G7167B), and an Agilent 6550 iFunnel Q-TOF mass spectrometer (G6550A). Extracted metabolites were separated on an Acquity UPLC HSS T3 Column (1.8 µm×2.1 mm, 150 mm) (Waters, Milford, MA). B. Injection volume was 2 µL for each cecal content sample and 5 µL for each serum

sample, both stored at 10 ºC. QTOF analysis was operated in electrospray ionization (ESI) in positive mode, with the following settings: capillary voltage, 3.5 kV; drying gas (nitrogen, 200 ºC) at a flow rate of 14 L/min; nebulizer gas (nitrogen), 40 psig; sheath gas (nitrogen, 300 ºC) at a flow rate of 12 L/min; MS1 mass range, m/z 60-1000; collision energy, 20 eV; acquisition rate of MS1, 2 spectra/sec. Vitamers were analyzed by liquid chromatography-tandem mass spectroscopy (LCMS/MS) whereas short chain fatty acids (SCFA) were analyzed by gas chromatography-tandem mass spectroscopy (GC-MS/MS)

SFCAs in feces or cecal content were quantified using a GC-MS based assay as described in Zheng et al (doi: 10.1007/s11306-013-0500-6) with slight modifications. In brief, for each feces sample, 40 mg was aliquot and was added with 0.005 M sodium hydroxide solution containing deuterated SCFAs as internal standards, namely 50 µg/mL d4-acetate, 10 µg/mL d2-propionate, and 10 µg/mL d2-butyrate. The sample was homogenized on a TissueLyzer (Qiagen, Hilden, Germany) and then centrifuged at 13,200 rpm for 20 min. The supernatant layer was transferred to glass tubes and derivatized by subsequently adding water, 1-propanol:pyridine (3:2, v/v), and propyl chloroformate, followed by 2-min sonication. The propyl derivatives were extracted twice with hexane and the combined extracts were transferred to anhydrous sodium sulfate-containing autosampler vial upon GC-MS analysis. The instrumental analysis was conducted using an Agilent 7820A GC-5977B single quadrupole MSD system installed with an electron ionization source (Santa Clara, CA, USA). One µL of extracted was injected under 1:10 split mode, vaporized, and the analytes were separated by an

Agilent DB-5 column (30 m x 0.25 mm x 0.25 µm) (Santa Clara, CA, USA) with helium flowing through at 1 mL/min as the carrier gas. The following temperature program was used: initial oven temperature held at 50 ºC for 2 min, ramped to 70 ºC by 10 ºC/min, to 85 ºC by 3 ºC/min, to 110 ºC by 5 ºC/min, to 290 ºC by 30 ºC/min, and finally maintained at 290 ºC for 8 min.

Supplemental Figure 1

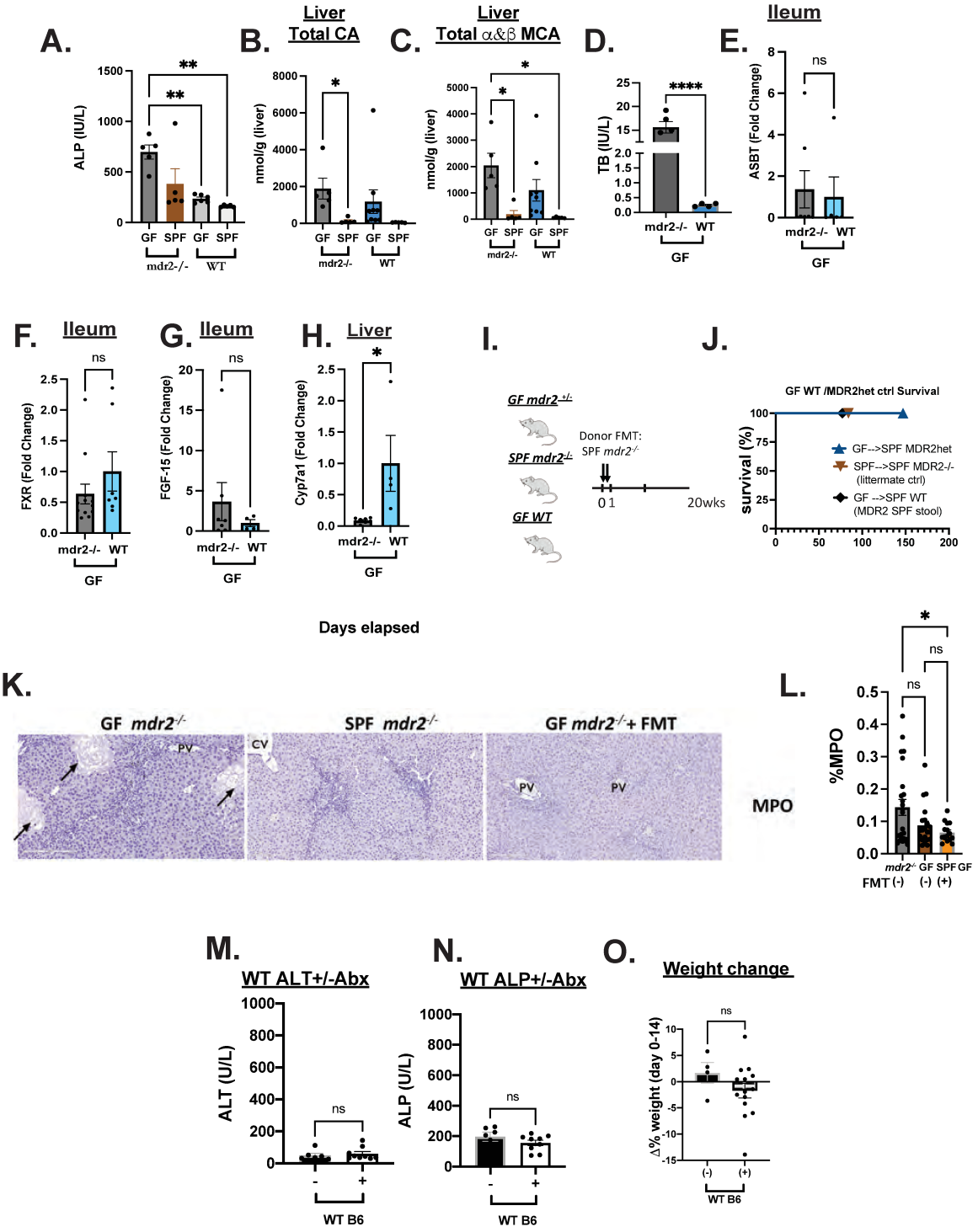

Supplemental Figure 2

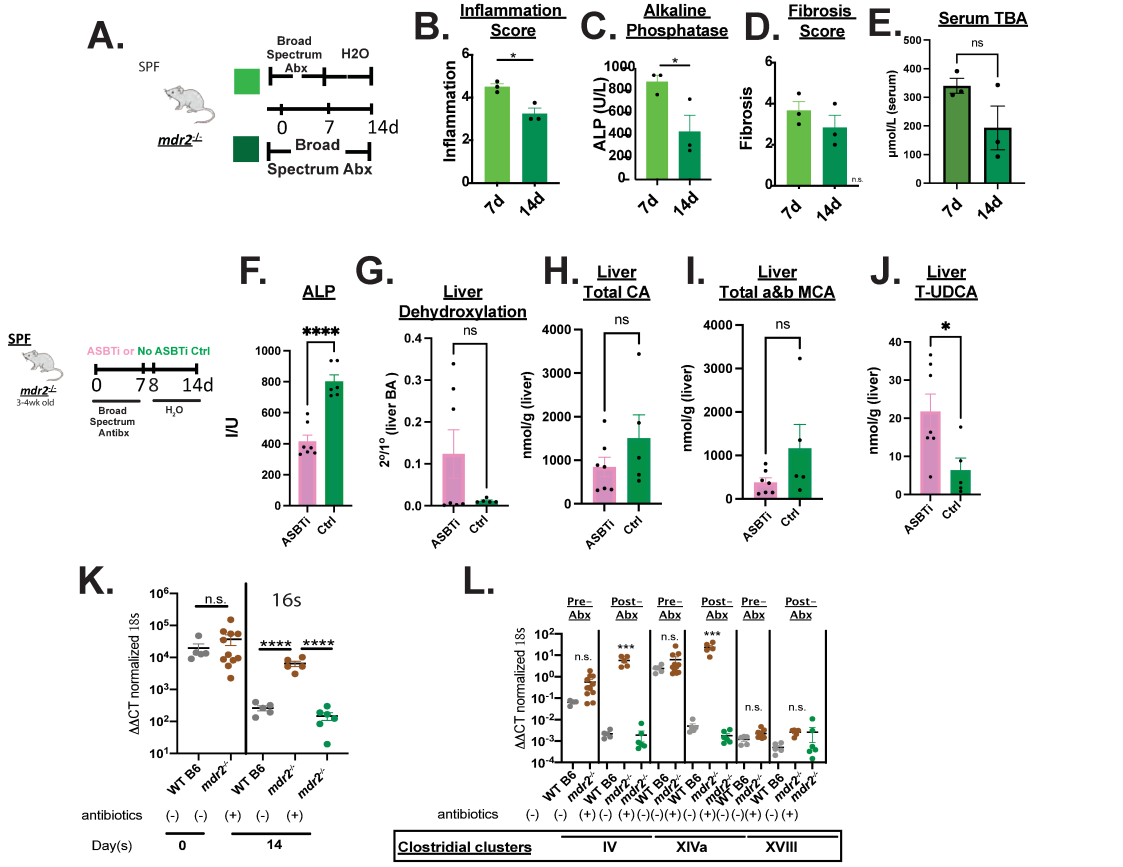

Supplementary Figure 3

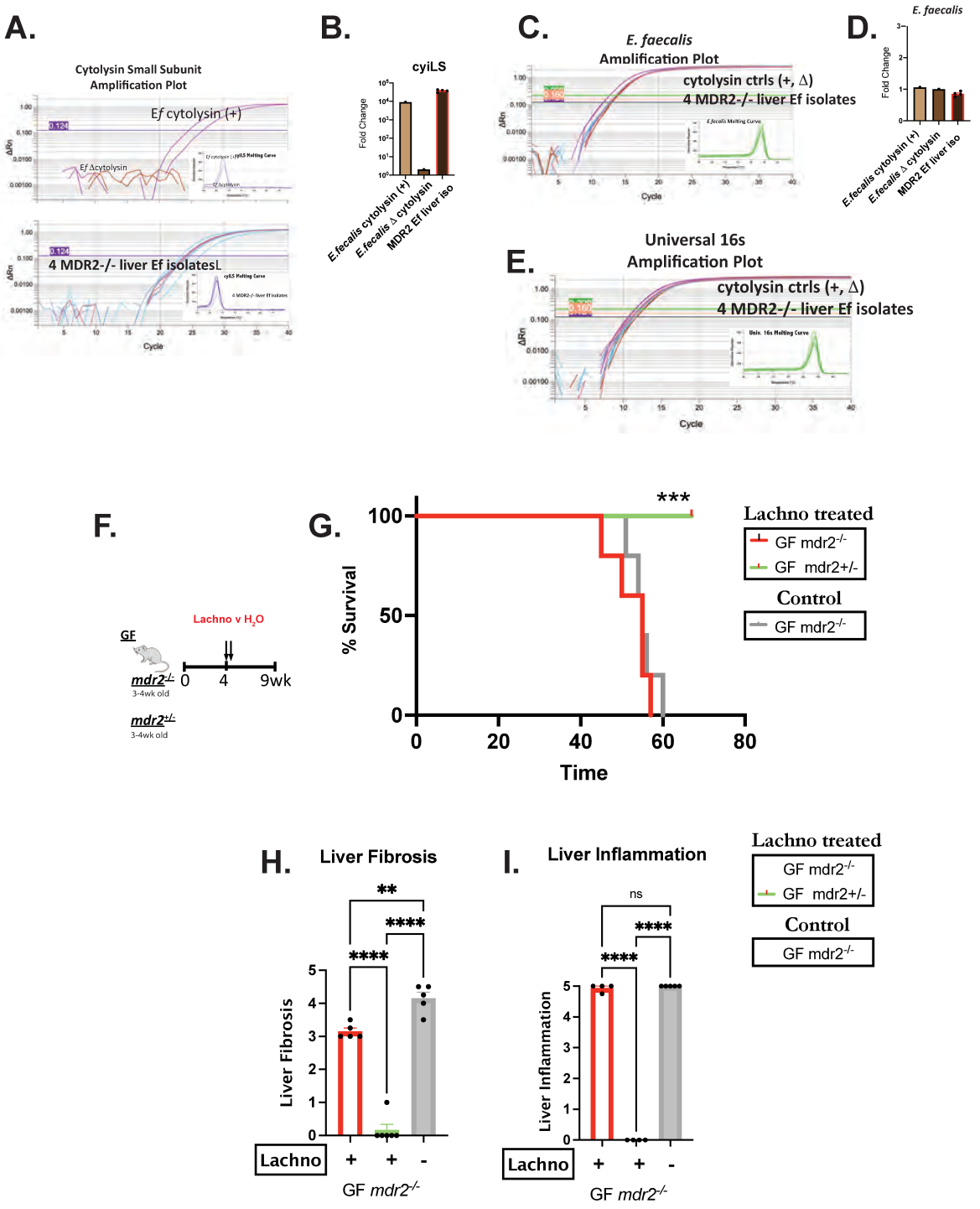

Table S1: Primers for qPCR

Taqman Probes (mouse)	Cat #	
MCP-1	Mm00441242_m1	
Lcn-2	Mm01324470_m1	
Col1a1	Mm00801666_g1	
TIMP-1	Mm01341361_m1	
SYBR green primers (mouse)	**Forward**	**Reverse**
iNOS2	GTGTTCCACCAGGAGATGTTG	CTCCTGCCCACTGAGTTCGTC
IL-6	AGTTGCCTTCTTGGGACTGA	TCCACGATTTCCCAGAGAAC
TNF-a	CTGGGACAGTGACCTGGACT	GCACCTCAGGGAAGAGTCTG
18s	ggtaacccgttgaaccccat	caacgcaagcttatgacccg

18s was used as reference gene. MCP-1, Monocyte Chemoattractant Protein-1; Lcn-2, Lipocalin-2; Col1a1, collagen 1a1; Timp1, tissue inhibitor of metalloproteinases 1; iNos-2, inducible nitric oxide-2; IL-6, Interleukin-6; TNF-a, Tumor Necrosis Factor-alpha.

Supplemental Figure 1: Characteristics of GF/ SPF *mdr2*$^{-/-}$ and WT mice with and without broad-spectrum antibiotics. Akaline phosphatase (ALP), total cholic acid (CA) and α&β murichlolic acid (MCA) in GF v SPF in 6-8wk old *mdr2*$^{-/-}$ and WT mice (A-C). Pooled serum TB, ileal expression of apical sodium dependent bile acid transporter (ASBT), farsenoid-X receptor (FXR), fibroblast growth factor 15 (FGF-15), along with liver cyp7a1 in GF *mdr2*$^{-/-}$ vs WT mice (D-H). Survival in untreated SPF WT and *mdr2*$^{-/-}$ mice (WT= 13, *mdr2*$^{-/-}$ 23) (I-J). Representative photomicrographs of 6-8wk old GF, SPF, or post-FMT GF mdr2-/- murine liver stained by myeloperoxidase (MPO) (K, 100X) along with composite automated scoring of % MPO positive cells (L). Serum ALT (M), ALP(N) and 14d change in weight (O) following broad-spectrum antibiotics (vancomycin, neomycin and metronidazole) ad libitum compared to water controls. Results are expressed as means +/- SEM. Survival data analyzed by Log-rank (Mantel-Cox) test, group or pairwise comparisons performed by ANOVA or Student t-test, respectively. PCoA of the beta were analyzed by permanova analysis. P-value*P < .05, **P < .01, ***P <.001, ****P < .0001.

Supplemental Figure 2: Efficacy of putative hepatoprotective resident bacteria in *mdr2*$^{-/-}$ mice. Experimental design of accelerated antibiotic treatment model: SPF *mdr2*$^{-/-}$ mice were treated with broad-spectrum antibiotics (vancomycin, metronidazole and neomycin) for 7d vs. 14d (A) resulting in aggressive liver inflammation and injury: the 7d antibiotic regimen had increased histologic inflammation (B) and serum alkaline phosphatase (C), but not liver fibrosis (D), and increasing trend of serum total bile acids (E) (7d, N=3, 14d, N=3, 2 experiments). Experimental design of ad libitum exposure in drinking H2O of ASBT inhibitor (GSK23306,10mg/kg) for 14d in setting of 7d broad antibiotic pretreatment in 4–5-week-old SPF mdr2-/- mice vs no ASBTi group (N=5-7mice/group). Effect of ASBT inhibition on: alkaline phosphatase (F), Liver dehydxylation ratio (total secondary/primary liver BA) (G), total liver cholic acid (H), total liver α&β muricholic acid (MCA)(I), and liver taurine conjugated ursodiol

(UDCA) (J). *q*PCR amplified results of fecal samples from *mdr2*$^{-/-}$ mice with and without broad-spectrum antibiotics (vancomycin, neomycin, and metronidazole) using the 16s (K) and Clostridial cluster primers (cluster IV, XIVa, and XVIII) (L) normalized to 18s. Experimental desi3n of treatment of 3-4wk old SPF *mdr2*$^{-/-}$ mice treated with 7 day treatment of broad antibiotic cocktail followed by a 1d washout period, then the inoculation of 17-strain of Clostridium (M) and assessing 14 weight change (N), ALP & ALT (O-P). (n=4 mice in each treatment and control groups). Following Lachnospiraceae treatment of *mdr2*$^{-/-}$ mice outlined in Fig4E (lachno, N=13, H2O ctrl, N=12), we assessed pooled data from 2 separate experiments of ALT (Q) and total BA (R). qPCR assessment of orphan receptor FXR pathway by look at liver cyp7a1 (S), ileal FGF15 (T), fecal TBA (U), and fecal *bsh* activity (ratio of total unconjugated/conjugated fecal BA), (V) in *mdr2*$^{-/-}$ exposed to Lachnospiraceae. Group or pairwise comparisons performed by ANOVA or Student t-test, respectively. *P < .05, **P < .01, ***P <.001, ****P < .0001.

Supplemental Figure 3: Comparison of amplification and melt curves of DNA isolated from E. faecalis translocated *mdr2*$^{-/-}$ murine liver isolates from four different *mdr2*$^{-/-}$ mice by assessing small cytolysin subunits, cylLS, genomic DNA along with experiements on effect of Lachnospiraceae reconstitution in GF mdr2$^{-/-}$ mice. . E. faecalis cytolysin+ strain and deletion cytolysin mutant from the Schnabl lab were used as controls. Fold change (relative to Ef null control) of cylLS (A-D). Melting curve and amplification curves of control E. faecalis rpoB and Universal 16s primers of controls and murine E. faecalis isolates (E). Experiment design (F) and Kaplan-Meyer survival curves (G) of orally inoculated GF mdr2-/- or mdr2+/- mice with 10^8 of 21-strain Lachnospiraceae (Lachno) or H2O controls in (H2O, N=5, Lachno, N=4/group) and measure histologic hepatic fibrosis and inflammation(C-D).

Deleted: along with experiements on effect of Lachnospiraceae reconstitu

Formatted: Superscript

Formatted: Superscript

Deleted: ¶

Group or pairwise comparisons performed by ANOVA or Student t-test, respectively. *P < .05, **P < .01, ***P <.001, ****P < .0001.

Table S1: Primers for qPCR

List of primers utilized in study.